Research Square

Preprints are preliminary reports that have not undergone peer review.
They should not be considered conclusive, used to inform clinical practice,
or referenced by the media as validated information.

An Lsr2-like xenogeneic silencer confers immunity against AT-rich bacteriophage infection

Julia Frunzke

j.frunzke@fz-juelich.de

Forschungszentrum Julich https://orcid.org/0000-0001-6209-7950

Biel Badia Roigé

Forschungszentrum Julich

Nadiia Pozhydaieva

TU Delft

Ombeline Rossier

Université Paris-Saclay https://orcid.org/0000-0003-4987-1811

Konstantinos Kalogeropoulos

Technical University of Denmark https://orcid.org/0000-0003-3907-9281

Christophe Regeard

Université Paris-Saclay

Stan Brouns

Delft University of Technology

Eugen Pfeifer

Micalis Institute https://orcid.org/0000-0002-4554-3696

Article

Keywords:

Posted Date: May 5th, 2026

DOI: https://doi.org/10.21203/rs.3.rs-9446490/v1

License: This work is licensed under a Creative Commons Attribution 4.0 International License.
Read Full License

Additional Declarations: There is **NO** Competing Interest.

An Lsr2-like xenogeneic silencer confers immunity against AT-rich bacteriophage infection

Biel Badia Roigé[a,b], Nadiia Pozhydaieva[c,d], Ombeline Rossier[e], Konstantinos Kalogeropoulos[c,d,f,g], Christophe Regeard[e], Karen L. Maxwell[h], Stan J. J. Brouns[c,d], Eugen Pfeifer[i,j], Julia Frunzke[a,b*]

[a]Institute of Bio- und Geosciences, IBG-1: Biotechnology, Forschungszentrum Jülich, Jülich, Germany

[b]HHU Düsseldorf, Faculty of Mathematics and Natural Sciences Institute of Microbial Interactions, Heinrich-Heine-University Düsseldorf, Düsseldorf, Germany

[c]Department of Bionanoscience, Delft University of Technology, The Netherlands

[d]Kavli Institute of Nanoscience, 2629 HZ Delft, The Netherlands

[e]Université Paris-Saclay, CEA, CNRS, Institute for Integrative Biology of the Cell (I2BC), 91198, Gif-sur-Yvette, France

[f]Department of Biotechnology and Biomedicine, Technical University of Denmark, Denmark

[g]Center for Translational Protein Design, Technical University of Denmark, Søltofts Plads, DK-2800, Kongens Lyngby, Denmark

[h]Department of Biochemistry, University of Toronto, Toronto, Ontario, Canada

[i]Université Paris-Saclay, INRAE, AgroParisTech, MICALIS, 78350 Jouy-en-Josas, France

[j]Université Paris-Saclay, INRAE, MetaGenoPolis, 78350 Jouy-en-Josas, France

*Corresponding author: Julia Frunzke (j.frunzke@fz-juelich.de)

Abstract:

Lsr2-like xenogeneic silencers are widespread nucleoid-associated proteins in Actinomycetota and are encoded by diverse bacteriophages. However, their roles during bacteriophage infection, one of the most direct encounters with foreign DNA, remain unexplored. In *Corynebacterium glutamicum*, the Lsr2-like protein CgpS is encoded within the mobile genetic element CGP3 and is known to silence transcription of foreign DNA within this region. Here we show that CgpS restricts infection by the AT-rich bacteriophage JeanGrey. Upon phage DNA injection, CgpS binds phage-derived AT-rich sequences and represses early phage gene transcription. This transcriptional bottleneck prevents efficient phage genome replication and delays progression of the viral program. The resulting temporal window enables activation of host stress and defense pathways, including LexA-regulated SOS genes and antiviral systems. Our findings reveal a novel antiviral function for an Lsr2-like silencer and suggest that xenogeneic silencers can act as regulatory barriers that modulate the outcome of phage infection in Actinomycetota.

Introduction:

Bacteria are continuously exposed to foreign DNA[1], an evolutionary force shaping their genome[2] and cellular physiology[3]. This genetic material commonly arrives in form of plasmids, mobile genetic elements (MGEs), or in infectious viral particles, known as bacteriophages[4,5] or phages. While these interactions can provide adaptive traits[1], they also carry substantial risks like uncontrolled high transcription of foreign genes, which can lead to toxicity, increased metabolic burden, and, in the case of viral infections, cell death[6,7]. To mitigate these threats, bacteria have evolved diverse strategies to recognize incoming DNA followed by its degradation or silencing. Bacteriophage infections have driven a long-standing co-evolutionary arms race, giving rise to a wide range of antiphage defense systems and, reciprocally, corresponding phage-encoded countermeasures[5,8,9]. This dynamic interplay has garnered increasing attention in recent years, driven by the interest in the therapeutic and biotechnological potential of phage-based applications[10-12].

Once phage DNA enters a host cell, bacteria can resist infection in different ways. Some strategies, such as abortive infection, sacrifice the infected cell to protect the community, while others, like CRISPR-Cas and restriction-modification (RM) systems, degrade incoming DNA to allow survival of the infected cell[13]. An alternative to these destructive strategies that also facilitates the tolerance of foreign DNA and its integration into host regulatory circuits relies on xenogeneic silencers (XSs). They are nucleoid-associated proteins that preferentially bind AT-rich foreign sequences[14], oligomerize across promoters and intergenic regions, and hinder transcription[15,16]. XS proteins are widespread, including H-NS in Proteobacteria[17], Rok in Firmicutes[18], and Lsr2 in Actinomycetota[19], and can even be found encoded by phages, belonging to the most abundant regulators in actinobacteriophages[20,21]. Despite their overarching key role in silencing foreign DNA, several recent studies hint towards a functional diversity that remains incompletely elucidated.

Lsr2 proteins are widespread in Actinomycetota[22-24]. These proteins share a common architecture consisting of an N-terminal oligomerization domain and a C-terminal DNA-binding domain, enabling cooperative binding across extended AT-rich sequences[25-27]. In *Mycobacterium*, Lsr2 functions as a global regulator for cell wall biosynthesis and controls the expression of virulence clusters[28]. In some species, such as *M. smegmatis,* it also acts as a cyclic-di-GMP receptor, promoting keto-mycolic acid synthesis and biofilm formation[29]. In *Streptomyces*, Lsr2 similarly binds AT-rich DNA, represses horizontally acquired and specialized metabolic gene clusters, including cryptic antibiotic biosynthetic pathways[22,30]. Lsr2 has further been shown to interact with related homologues, such as LsrL, thereby modulating chromatin organization and transcriptional control[31]. Collectively, these roles illustrate a functional versatility that extends far beyond simple xenogeneic silencing.

In *Corynebacterium glutamicum* ATCC 13032, the Lsr2-like protein CgpS is encoded within CGP3, a 187 kb mobile genetic element[24,27] rich in AT-sequences that is capable to excise upon DNA damage[32]. Together with other cryptic prophage elements, this large element was deleted to generate the genome-reduced industrial platform strain MB001[33]. CGP3 comprises more than 150 mostly uncharacterized genes, including an active RM system (cg1996-98)[34]. In previous work, we demonstrated that CgpS represses transcription across most of the CGP3 element that encodes it, while exhibiting only limited and non-functional binding to AT-rich sequences within the host genome[27]. Nevertheless, given the broad spectrum of functions described for Lsr2-like silencers in other organisms, additional roles for CgpS beyond xenogeneic silencing cannot be excluded. Given their widespread abundance in host and (pro)phage genomes, we hypothesize that these proteins might also play a role in innate immunity upon infection with phages carrying a AT-rich genome[35].

Here, we demonstrate that the CGP3-encoded Lsr2-like silencer CgpS functions as an antiviral factor in *C. glutamicum* ATCC 13032 by targeting incoming AT-rich phage DNA. CgpS binds and oligomerizes on invading genomes, repressing early phage transcription and thereby preventing productive replication. We further propose that CgpS can transiently re-localize from chromosomal sites to incoming DNA, establishing an immediate silencing barrier upon infection. This redistribution delays phage development and enables a coordinated activation of host defense pathways, including the SOS response. To place these observations in a broader evolutionary context, we extended our analysis by examining the distribution and genomic regions of Lsr2 homologues across corynebacterial lineages, identifying numerous host-encoded variants as well as homologues associated with plasmids and putative integrative conjugative elements (ICEs). Integrating multi-omics, biochemical, and functional analyses, we uncover a previously unrecognized antiviral role for Lsr2-like proteins and expand the functional landscape of xenogeneic silencing in Actinomycetota.

Results:

CGP3-encoded Lsr2-like protein confers phage resistance

CgpS is an Lsr2-like xenogeneic silencer encoded within the mobile genetic element CGP3 and is known to preferentially bind AT-rich DNA. Based on this property, we hypothesized that CgpS may also recognize and bind incoming phage genomes with high AT content. To determine whether the CGP3-encoded Lsr2-like protein CgpS influences phage susceptibility, we screened a panel of corynephages (CL31[36], PSonyx[37], and JeanGrey (Supplementary Fig. 1,a)) on *C. glutamicum* strains differing in their CGP3 backgrounds. We tested infection in the wild-type *C. glutamicum* ATCC 13032 and, to avoid masking effects of the CGP3-encoded RM system (cg1996-98), which provides broad phage resistance, we compared a CGP3-positive strain lacking the RM system (hereafter +CGP3) with the prophage- and CGP3-free strain MB001[33] (-CGP3). The AT-rich phage JeanGrey (46% GC content), which encodes multiple DNA hypermodification genes (Supplementary Table 3), produced progeny only in-CGP3, whereas +CGP3 (and WT) showed no culture collapse but instead displayed a transiently elongated cellular morphology without lysis (Fig. 1b). In contrast, phage CL31 (54.4% GC content) lysed all strains except the wild type approximately 120 min after adsorption, and PSonyx (53% GC content) impaired growth in both +CGP3 and-CGP3, albeit less efficiently than CL31 (Supplementary Fig. 1,b). In both cases, resistance in *C. glutamicum* primarily depended on the CGP3-encoded RM system.

To identify possible CGP3-encoded elements responsible for the resistance phenotype observed with JeanGrey, we generated a deletion library in the +CGP3 background in which defined segments of the element were systematically removed. Despite these deletions, the AT-rich phage JeanGrey infected only the-CGP3 strain. None of the smaller 10 kb deletions (D1–D20, Fig. 1,a) altered the resistant phenotype (Fig. 1,b). CgpS was the only element retained in the deletion library due to its essential regulatory role within the CGP3 region[27].

As CgpS is also autoregulated via self-silencing and its cellular abundance scales with the burden of AT-rich DNA, its presence remained unchanged in all deletion strains. Overexpression of *cgpS* in the-CGP3 background resulted in severe growth impairment, likely due to nonspecific binding across the chromosome, and therefore ruled out the performance of reliable infection assays. Re-integration of an autoregulated copy of *cgpS* into the-CGP3 strain showed a 4-fold reduction of *cgpS* transcript levels in comparison with the WT, as determined by RT-qPCR (Supplementary Fig. 1,c). This further confirms its autoregulatory dynamics. Therefore, expression levels are determined by the amount of AT rich DNA targets.

To modulate CgpS abundance and assess the contribution of CGP3-encoded elements to phage infection, we generated a large deletion mutant (Δ70%) designed to reduce the amount of CgpS target DNA and thereby lower basal CgpS levels prior to infection. While none of the previously

tested 10 kb deletions affected susceptibility to JeanGrey, infection by the phage was restored in the Δ70% background (Fig. 1,b). These observations are consistent with CgpS acting as the primary factor mediating resistance and suggest that the amount of XS target DNA modulates this effect.

CgpS blocks an early stage of the phage life cycle

To test the hypothesis that CgpS mediates early phage gene silencing, we characterized the infection cycle of the previously unstudied phage JeanGrey by monitoring adsorption, phage genome replication, transcription, and protein synthesis in the +CGP3 and -CGP3 strains. Adsorption, quantified by free phage counts during the first 90 min of cultivation, was comparable between strains (Fig. 1,c). However, in-CGP3, phage progeny was produced, and lysis began after ~120 min, whereas +CGP3 showed a continuous decline in free phage titers. qPCR analysis of intracellular phage DNA relative to host genomic DNA revealed robust genome replication in-CGP3 but no detectable replication in +CGP3. In the latter, phage DNA levels remained below the detection limit (Fig. 1,c), reflecting dilution of the phage signal by increasing host DNA in the absence of phage genome amplification. These observations indicate that phage DNA is injected into both strains but does not replicate in the presence of CgpS.

Transcriptomic analyses supported a block in productive infection. Both strains expressed early phage genes involved in DNA metabolism, although transcript levels were markedly reduced in +CGP3. The broad transcriptional signal detected at 15 min post-infection reveals that the JeanGrey genome is fully injected at this time point. In-CGP3, infection progressed with strong induction of structural and lysis genes, culminating in transcriptional takeover of the cell (Fig. 1,d). In contrast, late gene expression was absent in +CGP3, consistent with a block in productive infection.

Proteomic analysis of the first 60 min of infection further corroborated these findings. Extensive phage proteome coverage was observed exclusively in -CGP3, with 80% of the predicted phage proteome detected, whereas +CGP3 showed only limited detection of proteins corresponding to early gene expression, together with residual structural proteins likely derived from adsorbed phage particles (29% of the predicted phage genome)(Fig. 1,e and Supplementary Fig. 1,d). Successful host takeover in -CGP3 was further reflected in the global proteomic signal. The total fraction of the signal in proteomics experiment contributed by phage proteins increased from 0% to approximately 4% of total detected signal within the first 60 min of infection. In contrast, for infection of +CGP3, the phage contributed signal fraction was only ~0.5% after 30 min of infection and slightly declined to ~0.2% at 60 min (Supplementary Fig. 1,e), consistent with a failed infection cycle.

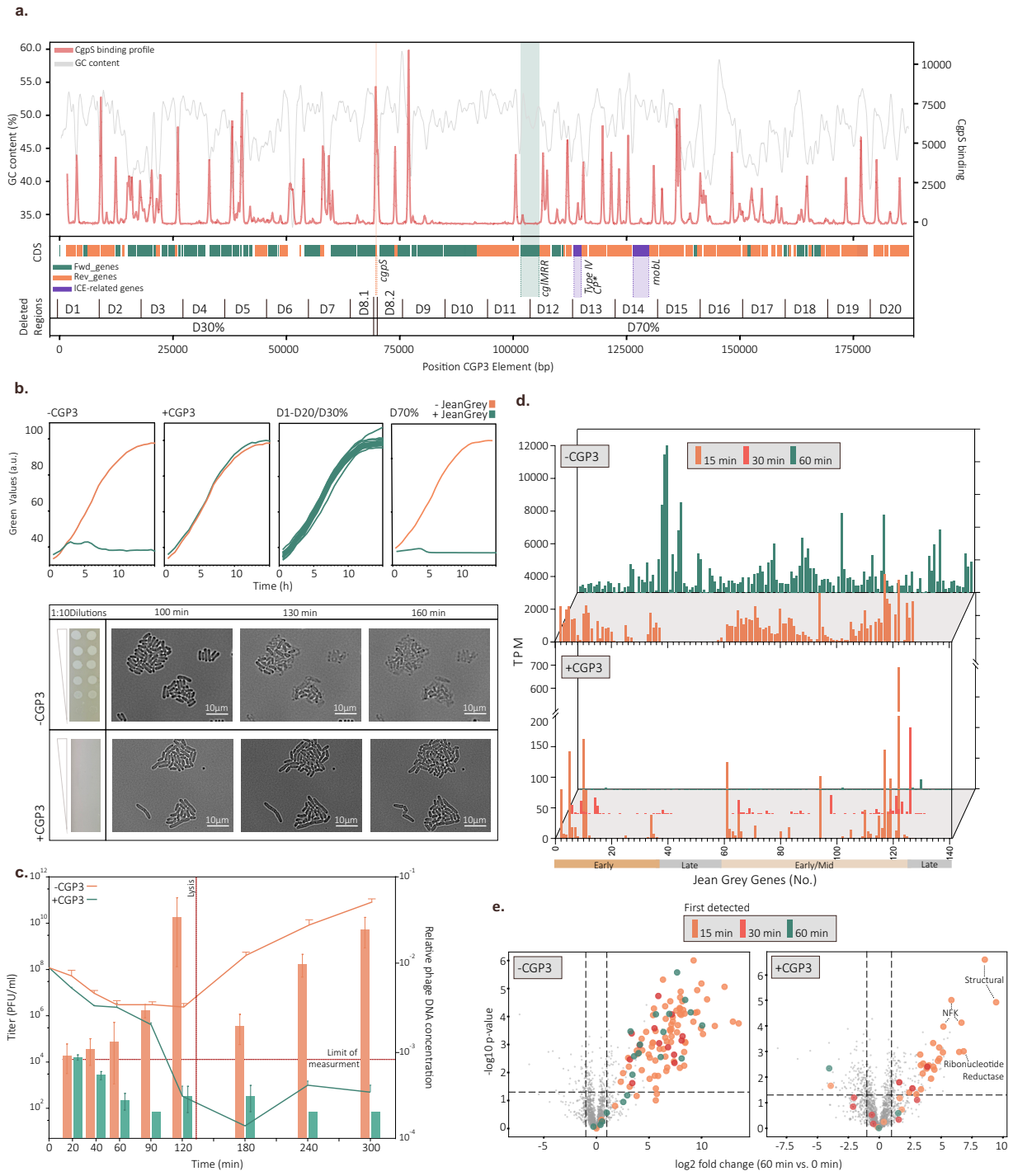

Fig. 1 | The Lsr2-like protein CgpS encoded within the CGP3 mobile genetic element restricts bacteriophage JeanGrey infection after DNA injection. (a) Genomic overview of the CGP3 element. The CgpS ChAP-seq binding profile is shown in red and GC content in grey. Local decreases in GC content coincide with DNA peaks of CgpS enrichment. Coding sequences (CDSs) are shown in green (forward strand) and orange (reverse strand). Genes associated with an integrative and conjugative element (ICE) are highlighted in purple. Key annotated features include *cgpS*, the CGP3 restriction–modification system (*cglMMR*), a truncated type IV conjugative protein (asterisk), and the relaxase *mobL*. The deleted regions covered by the CGP3 deletion library are indicated. (b) Phage infection screening of the CGP3 deletion library together with -CGP3 and +CGP3 strains (n=2; mean value); orange without phage, green indicates infected samples. Lysis phenotypes were further validated by serial dilution spot assays on -CGP3 and +CGP3 strains and

by live cell imaging of infected cultures at 100, 130, and, 160 min. Scale bar, 10µm. (c) Infection dynamics of JeanGrey in-CGP3 and +CGP3 backgrounds. Lines represent phage titers (Left axis) and they were determined by dilution spot assays (n=3 biological replicates; mean ± SD). Bars represent mean relative phage DNA levels (Right axis) quantified by qPCR from three biological replicates and two technical replicates; error bars indicate SD. The qPCR detection limit, determined by the water control and the lowest phage DNA dilution control, is indicated by a red line. (d) RNA-seq analysis of phage transcripts at 15 and 60 min post infection in –CGP3 and at 15, 30, and 60 min in +CGP3. Differential expression analysis was performed using CLC Genomics Workbench (FDR p-value < 0.05; n = 2 biological replicates). Further statistical details are provided in the Methods. (e) Proteomic analysis of infected -CGP3 and +CGP3 cells at 15-, 30- and 60-min post infection. Log_2 fold changes represent differences in protein abundance between the initial time point (0 min) and 60 min post infection (Single values represented in Supplementary Fig. 2). Data points are color-coded according to the earliest time point at which each protein was detected: 15 min (orange), 30 min (red) and 60 min (green). Statistical significance was assessed using a two-tailed Student's t-test (p value < 0.05; n = 3 biological replicates; Further Information can be found in Supplementary Table 5).

Interaction of Lsr2-like CgpS with phage DNA reduces gene transcription

Cooperative binding of Lsr2-like proteins, like CgpS, requires local drops in GC content to recognize foreign DNA[24]. To assess whether CgpS can associate with and repress transcription of JeanGrey phage genes, we identified several AT-rich intergenic promoter regions with localized GC-content drops as putative CgpS binding sites (Fig. 2,a). Some candidate regions displaying characteristic GC-content dips (A–D, S1, and S2) were selected and tested by electrophoretic mobility shift assays (EMSAs) using ~200 bp fragments encompassing early phage gene promoters. Among these, regions A, S1, B, and D exhibited clear mobility shifts with increasing CgpS concentrations, indicative of direct protein-DNA interaction in vitro, whereas regions C and S2 showed no detectable shift (Fig. 2,b and Supplementary Fig. 3,a).

To validate interactions with the phage genomic regions B and D, we next performed chromatin affinity purification followed by sequencing (ChAP-Seq)[38]. As an initial approach, total DNA from cells infected at an MOI of 1 was sequenced 15 minutes post-infection using Illumina technology. However, this strategy yielded insufficient input phage genome coverage, detecting only sparse reads within the phage genome (Supplementary Fig. 3,b), whereas robust enrichment peaks within CGP3 confirmed proper execution of the protocol. These results indicate that the early stage of infection, prior to phage DNA replication, does not provide sufficient phage genetic material for reliable detection of CgpS binding events under our experimental conditions.

As an alternative approach to validate interaction in vivo, some of the EMSA-validated regions were cloned into a plasmid and subjected to ChAP-Seq, sequencing both input DNA and CgpS-enriched fractions (Fig. 2,b). This approach ensured sufficient and stable target DNA abundance while circumventing limitations caused by low phage DNA copy numbers and infection-induced cellular responses. The analysis confirmed enrichment of the tested B and D intergenic regions in the CgpS-bound fraction, whereas the negative control region *gntK* showed no enrichment (Fig. 2,b and Supplementary Fig. 3,c). This enrichment was further independently validated by qPCR (Supplementary Fig. 3,d). The input DNA control likewise exhibited no enrichment, confirming that

the observed peaks were specifically generated by CgpS binding. Notably, both regions displayed broad double peaks showing also interaction with the *mvenus* reporter gene, indicating that CgpS binding is not restricted to a single discrete site and may involve extended DNA condensation or looping[39,40].

To evaluate functional consequences in vivo, we used the plasmid constructs generated for ChAP–seq, in which candidate regions B and D were cloned upstream of an *mVenus* reporter in a low-copy plasmid system to assess CgpS-dependent transcriptional repression. Upon induction of *cgpS* expression, a pronounced relative reduction of respectively 30% and 40% in mVenus fluorescence signal was detected for both candidates, consistent with transcriptional downregulation or silencing by CgpS (Fig. 3,d).

To visualize potential relocalization of CgpS from chromosomal targets to invading phage DNA, we generated a construct containing a second autoregulated copy of *cgpS* fused to *mVenus* via a flexible linker. This strategy allowed incorporation of the tagged protein into native silencing complexes while preserving overall CgpS functional silencing. It must be noted that fusion of Lsr2-like proteins to autofluorescent proteins frequently affects oligomerization properties interfering with the silencing. Also in this case, the fusion construct caused a modest reduction in growth rate and minor morphological changes (data not shown). However, fluorescence microscopy revealed distinct single CgpS foci in the cells likely representing the CGP3-bound fraction of the XS protein. Nevertheless, some heterogeneity likely resulting from plasmid instability was detected. Phage particles were labeled with Alexa Fluor NHS ester to visualize capsids and identify infected cells. Using a microfluidics platform, cells were monitored during infection following phage addition. Upon cell exposure to JeanGrey, CgpS redistributed from defined chromosomal foci to sites corresponding to phage genome entry (Supplementary Fig. 4).

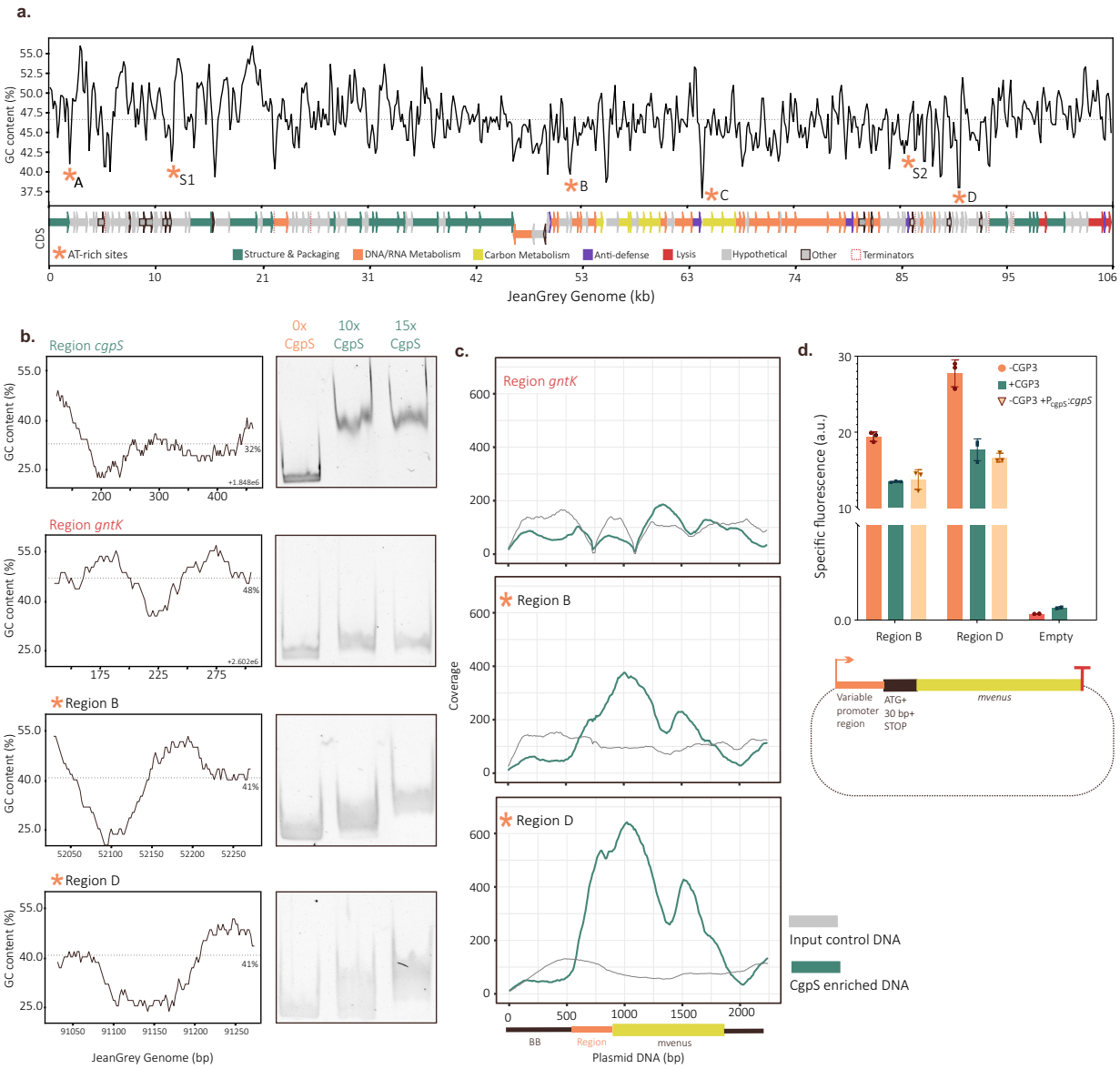

Fig. 2 | CgpS binding to phage promoter regions reduces gene expression. (a) Genome map of JeanGrey showing GC content (brown line) and annotated coding sequences (CDSs). Genes are color-coded by functional category: structural and packaging (green), nucleic acid metabolism (orange), carbon metabolism (yellow), putative anti-defense (purple), lysis (red), and hypothetical proteins (grey). Red dashed lines indicate transcriptional terminators. AT-rich regions selected for further analysis are marked with orange stars. (b) Electrophoretic mobility shift assays (EMSAs) of selected DNA regions. Genomic regions *gntK* and the native *cgpS* promoter region serve as negative and positive controls, respectively[27]. Regions B and D correspond to sites highlighted in (a). GC content profiles are shown, and DNA mobility shifts at increasing CgpS concentrations (0×, 10×, and 15× molar excess) are displayed to the right of each profile. (c) Plasmid-based ChAP-seq analysis of regions B and D in +CGP3 cells, with *gntK* as a negative control. Enriched DNA obtained from exponentially growing cells (4 h cultivation) following CgpS affinity purification (C-terminal Strep-tag inserted at the native *cgpS* locus) is shown in green, and input DNA is shown in grey. Below the enrichment plots a schematic of the plasmid construct is shown: backbone (brown), variable promoter region (orange), and fluorescent reporter gene (yellow). (d) Reporter assay assessing promoter activity in different strain backgrounds. A plasmid containing the variable promoter region (30 bp plus stop codon) fused to *mvenus* in the pJC1 backbone was introduced into *C. glutamicum*-CGP3 and +CGP3 strains. Empty vector includes only the *mvenus* without the promoter region (n=3; error bars indicate SD).

Phage-induced SOS and downstream immunity require CgpS-mediated silencing

The reduction in phage gene transcription and translation alone does not necessarily guarantee a successful defense outcome. We therefore hypothesized that CgpS-mediated silencing creates a window that enables activation of additional host responses required for survival. Initial microscopy of JeanGrey-infected +CGP3 cells revealed the presence of filamentous cells, resembling the stress-associated morphology induced by SOS activation following mitomycin C treatment[27]. This observation prompted us to compare the transcriptional responses of the two principal strains, +CGP3 and -CGP3, during the first 60 minutes of infection.

In -CGP3 cells, which support productive JeanGrey infection, no immediate host response was detected. At 15 minutes post-infection, transcriptional changes were minimal and primarily reflected modest upregulation of ribose and xylose transport systems. By 60 min post-infection, however, a broader metabolic shift became apparent, characterized by increased expression of genes involved in carbon uptake and utilization, including pathways for myo-inositol catabolism, citrate uptake, and methionine transport and metabolism. Notably, no induction of the known defense pathways or downstream SOS response genes were observed. Although *lexA* transcripts were reduced relative to non-infected controls, this decrease was not reflected at the protein level (Fig. 3,a and Supplementary Fig. 5), indicating that productive infection and rapid phage replication proceeds without triggering the activation of an effective protective stress and SOS-dependent defense response.

In contrast, +CGP3 samples exhibited a distinct transcriptional response upon phage infection. At 15 minutes post-infection, the +CGP3 strain showed pronounced upregulation of numerous defense-associated genes, including those encoding proteases, restriction endonucleases, components of the Wadjet system[41], and additional putative defense modules[42]. This activation coincided with the peak of phage gene transcripts detected at this time point. As phage transcript levels declined at 30- and 60-minutes post-infection, expression of these defense genes likewise decreased (Fig. 3,a).

Many of the early upregulated genes in +CGP3 infection are known to be repressed by LexA. Consistent with activation of the SOS regulon, *recA* transcript levels were increased and reflected at the protein level. Elevated RecA promotes autoproteolysis of the LexA repressor[43], leading to induction of LexA-repressed genes, as observed in the transcriptomic data, including *recX*, *recA*, the putative ATP-dependent protease *radA*, a DNA repair exonuclease (cg1318), and the cell division suppressor *divS*[44] (cg2113). Increased abundance of several of these gene products was further supported by proteomic analysis. Nevertheless, further degradation of cleaved LexA fragments was not detected at the protein level during the 60 min time window (Fig. 3,a).

Interestingly, the elevated *divS* expression was detected alongside the pronounced filamentation observed in infected +CGP3 cells. To validate this response, we monitored fluorescence from a P_{divS} reporter driving production of the fluorescent protein Crimson during infection. Phage addition induced early reporter fluorescence in +CGP3 cells, confirming SOS activation, whereas-CGP3 cells lysed rapidly, preventing any measurable induction (Fig. 3,d).

Live-cell imaging further confirmed the morphological progression during infection. +CGP3 cells became markedly elongated between 130- and 150-minutes post-infection and subsequently fragmented into multiple daughter cells and resumption of growth (Supplementary Video 1 and 2).

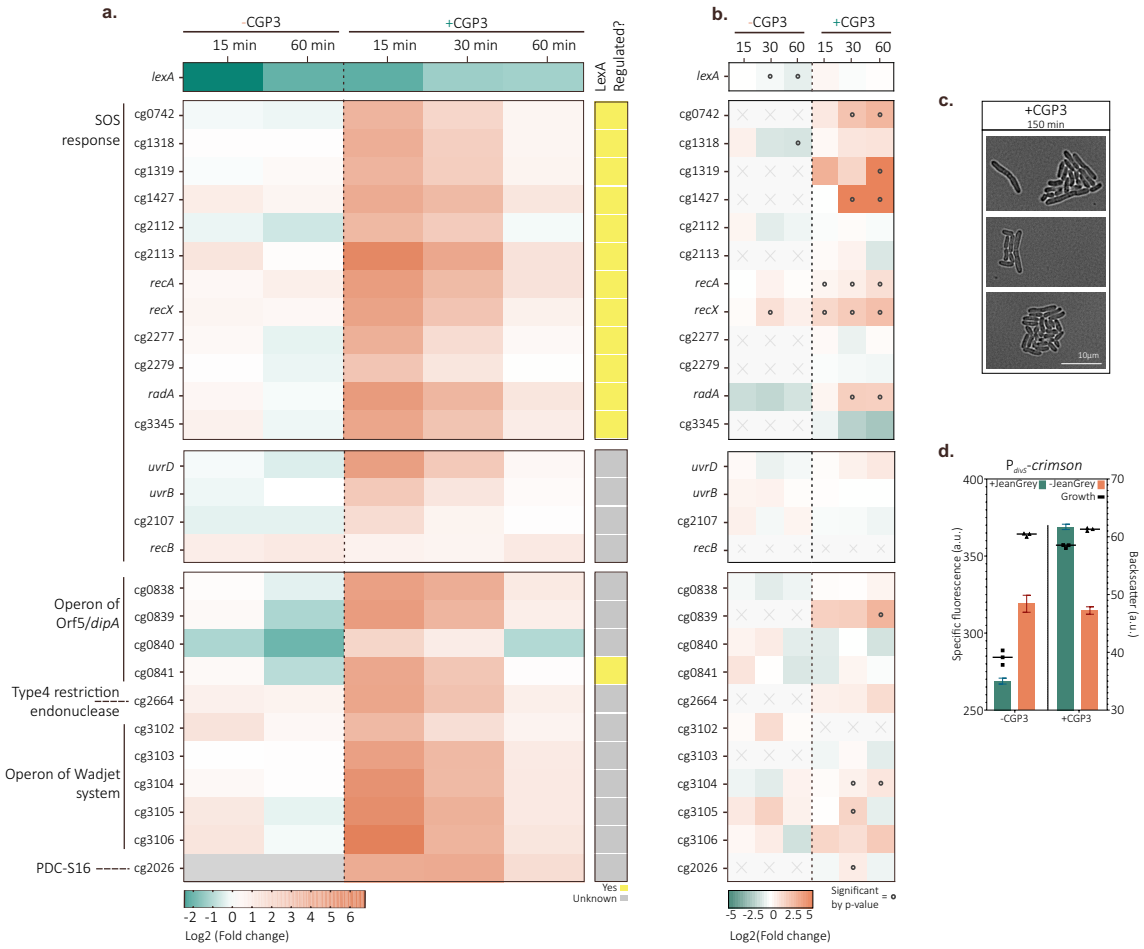

Fig. 3 | Transcriptomic and proteomic analyses reveal activation of an SOS-associated defense response in +CGP3 cells. (a) Transcriptomic profiling of genes associated with the LexA-regulated SOS response and defense systems in −CGP3 and +CGP3 backgrounds following JeanGrey infection. Timepoints: 15 and 60 min (−CGP3) and 15, 30, and 60 min (+CGP3). Genes predicted to be repressed by LexA are highlighted in yellow. All displayed genes meet the statistical significance threshold (false discovery rate (FDR) ≤ 0.05). FDR-adjusted P values were calculated in CLC Genomics Workbench using empirical analysis of differential gene expression (DEG). Data are derived from n = 2 biological replicates. Additional statistical details are provided in the Methods. (b)

Proteomic validation of transcriptomic changes. Fold changes in protein abundance are shown relative to time point 0. Although proteomic measurements are less sensitive and temporally delayed relative to RNA-seq, some proteins showing statistically significant differences between-CGP3 and +CGP3 were identified (two-tailed Student's t-test, $P < 0.05$; n = 3 biological replicates). (c) Morphology of +CGP3 cells 150 min after infection with JeanGrey. Cells display an elongated phenotype without detectable lysis. (d) Reporter assay for *divS* (cg2112) expression (n=3 ; bars indicate mean fluorescence intensity ± SD; black lines represent mean backscatter values).

Corynebacterial Lsr2 (CgpS) proteins are encoded by hosts and mobile genetic elements and form a distinct phylogenetic clade

Although the function of Lsr2-like proteins has been characterized in *Mycobacterium*[25,29] and *Streptomyces*[22,31], their broader evolutionary functional distribution remains unclear. Dulberger et al. demonstrated that Lsr2 proteins of mycobacteriophages are phylogenetically distinct from those found in mycobacterial host genomes[45]. To position CgpS within this landscape, we performed a comprehensive phylogenetic analysis of Lsr2-like proteins across Actinomycetota-infecting phages[46], recent *C. glutamicum* isolates, and also including selected mycobacterial representing hosts[45]. We computed a phylogenetic tree from the protein sequence alignment and found a robust and clear clade separation between corynebacterial and other Lsr2 proteins (Supplementary Fig. 6).

To further resolve the position of CgpS within the Lsr2 phylogenetic tree, we focused on the corynebacterial part of the tree. Within this group, CgpS in *C. glutamicum* segregated together with a homolog of *C. suranareeae* (NZ_AP017369) from other chromosomal Lsr2 homologs, forming a distinct well-supported sub-branch (Fig. 4,a). Given that CgpS is encoded within CGP3, we examined the genomic neighborhoods of Lsr2 homologs from the corynebacterial branch and compared them to Lsr2 regions of mycobacterial genomes. For this, we extracted 180 regions, including 50 genes up- and downstream of *cgpS*/*lsr2* (see Methods), compared their relatedness, and annotated them (Supplementary Table 9). We found that regions of *C. glutamicum* strains (i.e. CGP3) are highly conserved, and a nearly identical element is located in *C. suranareeae* (Fig. 4,bc). We noted that this region, and CGP3 encode T4CP (Type IV Coupling Protein) and Mob (Mobilization) proteins, which are required for conjugative transfer[47]. Moreover, T4CP of CGP3 is substantially shorter than of *C. suranareeae* indicating a truncation or frame shift event. We speculate that these regions are putative ICEs and that CGP3 is not capable of self-conjugative transfer. We found similar genetic patterns in an Lsr2-encoding plasmid of *C. comes* (NZ_CP046454 encodes a Mob), and in the *lsr2* region of *C. oculi* NML 130210 (NZ_LKST01000002 encodes Mob and T4CP). We also detected RM systems in these regions (Fig. 4b), and in total, 56 of the 180 analyzed *lsr2*/*cgpS* regions were predicted to harbor complete RM systems (Supplementary Table

9). Interestingly, although the *lsr2* region of *C. oculi* is AT-rich (4, d) like CGP3, they share no sequence homology (Fig. 4,c). Lastly, we could not find such patterns in *lsr2* regions that we extracted from mycobacterial genomes (Fig. 4,b).

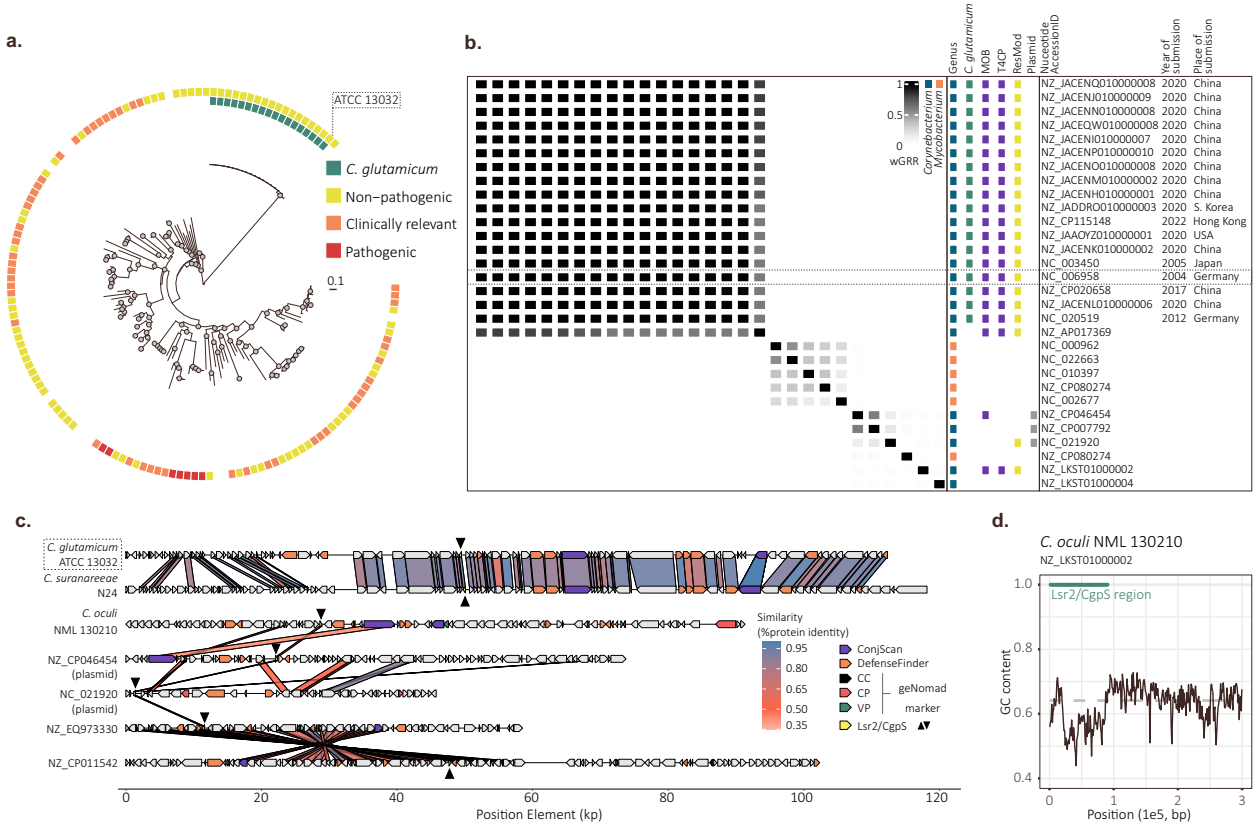

Fig. 4 | Phylogeny of Lsr2 proteins and their genomic context in Corynebacteria. (a) Phylogenetic tree of Lsr2 sequences retrieved from mycobacterial, phage and corynebacterial genomes (listed in Supplementary Table. 8). Protein sequences are aligned and used to compute a phylogenetic, midpoint rooted tree (Supplementary Fig. 6). The tree was then cut at the node separating corynebacterial sequences from the others. Bootstrap values (>70) are indicated by grey circles. Strains are classified according to pathogenic, clinically relevant, or non-pathogenic status[48-56]. (b) Weighted Gene Repertoire Relatedness (wGRR) matrix of Lsr2-associated regions (Lsr2 ± 50 genes) with accompanying metadata (nucleotide accession ID, year and location of sequence submission). Regions were extracted and annotated using models of ConjScan, DefenseFinder, and the database of geNomad. (c) Pairwise genome comparisons of selected regions from (b). Genes matching to profiles of ConjScan[47] are shown in purple, to profiles of DefenseFinder[42] in orange, and to profiles of *lsr2* in yellow (and black triangles). Matches to the geNomad[57] classifications are indicated as C (chromosomal), P (plasmid) and V (viral). (d) GC content of NZ_LKST01000002 (*C. oculi* NML 130210) with the *lsr2* associated region highlighted in blue/green.

Discussion

The discovery and characterization of antiviral defense systems specifically in Actinomycetota has lagged behind that in other bacterial phyla[58], in part due to the higher focus on Firmicutes and Proteobacteria as model systems. Consequently, genome-wide defense annotation in Actinomycetota frequently identifies a limited repertoire of well-characterized systems, predominantly restriction-modification modules, Wadjet systems, and CRISPR–Cas loci[42]. This apparent underrepresentation of novel defense mechanisms reflects the bias of the actual tools and limited experimental exploration. Direct functional investigation within the GC-rich actinobacterial species is therefore essential to uncover additional layers of phage resistance and to expand the current framework of bacterial innate immunity. In this study, we define an antiviral function for the ICE-encoded Lsr2-like xenogeneic silencer CgpS in *Corynebacterium glutamicum* ATCC 13032. CgpS restricts productive infection by the AT-rich bacteriophage JeanGrey by repressing early phage transcription and preventing the transition to genome replication and late gene expression. Rather than blocking genome entry or degrading the incoming DNA, CgpS imposes a transcriptional barrier that destabilizes the replicative cascade at its onset. This early interference generates a temporal window during which host-encoded stress and defense pathways become activated, thereby reshaping the outcome of infection (Fig. 5).

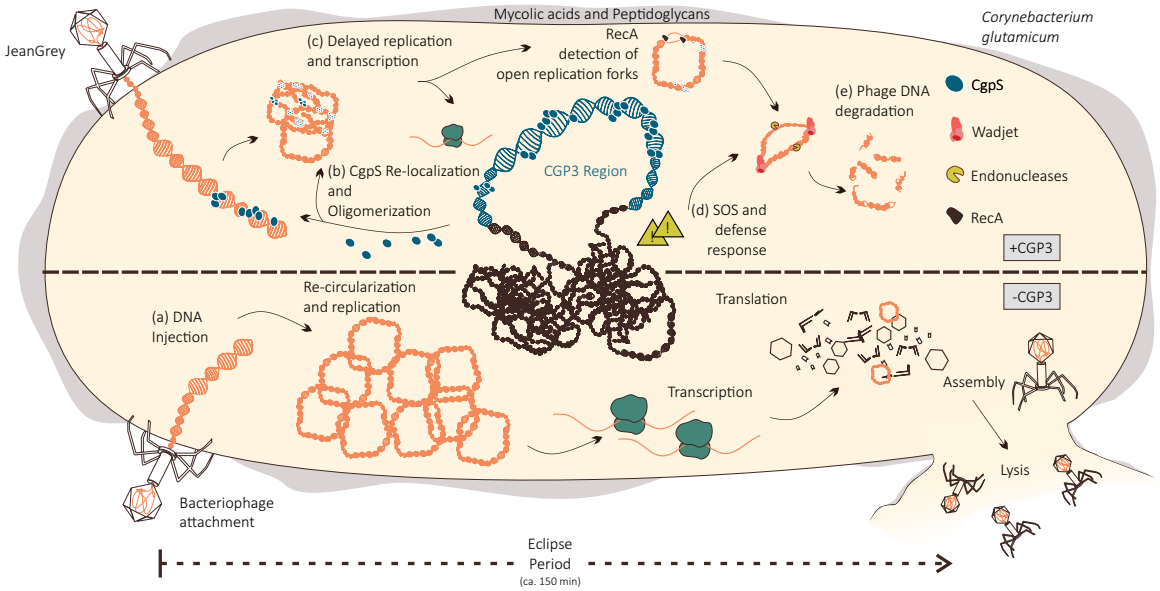

Fig. 5 | Model of the proposed role of the Lsr2-like protein CgpS in the defense against AT-rich phages. Schematic representation of the infection cycle of *C. glutamicum* challenged with JeanGrey. Under the tested conditions, the eclipse period from adsorption to first lysis is approximately 150min. In -CGP3 cells, phage infection proceeds to lysis within this timeframe. In contrast, in +CGP3 cells, phage DNA injection (a) is followed by rapid relocalization of CgpS (b) from the pre-existing cellular pool mostly bound to the CGP3 element. This interaction probably alters phage DNA conformation, silences early gene transcription and delays replication

(c). The extended infection cycle is proposed to create a temporal window that enables activation of host defense responses (d) and degradation of phage DNA (e). After ~150min, morphological features consistent with an SOS response are observed; however, cellular growth resumes.

The genomic architecture of JeanGrey, characterized by multiple local GC depressions and general AT rich content (Fig. 2), conforms to established binding preferences of Lsr2-like proteins[14]. In this context, CgpS functions as a cooperative DNA-binding factor that targets invading AT-rich sequences and restricts their transcriptional accessibility. This regulatory mode differs fundamentally from canonical DNA-degrading defense systems such as RM systems and CRISPR-Cas immunity. Rather than destroying foreign DNA, CgpS modulates its expression, thereby reshaping infection kinetics.

Detection of CgpS-phage DNA interactions in vivo is intrinsically constrained by the absence of phage genome amplification in +CGP3 cells (Supplementary Fig. 3). Phage DNA abundance at early stages depends on adsorption efficiency and the asynchronous nature of infection within the population. This may be also further reduced by downstream cellular responses. A plasmid-based system combined with ChAP-seq nevertheless provided evidence for interaction between natively expressed CgpS and phage-derived promoter regions. The broad peak architecture observed at these loci is consistent with cooperative binding and higher-order nucleoprotein assemblies[59]. However, xenogeneic silencing is not irreversible. Previous studies have demonstrated that competitive DNA binding, for example through utilization of transcription factors[60] or via employing catalytically inactive Cas proteins[61] to re-model the silencer-DNA complex, can partially relieve CgpS-mediated repression. These observations indicate that silencing of the foreign phage DNA would also depend on dynamic occupancy of target loci and may be susceptible to antagonistic DNA-binding factors.

Xenogeneic silencers have been proposed to represent functionally analogous systems to eukaryotic histones, as both mediate DNA condensation and transcriptional control[15]. Histone-mediated condensation of HSV viral DNA has recently been described as a transcriptional restriction mechanism in eukaryotic cells[62,63]. This functional parallel raises the possibility that chromatin-based interference represents a conserved principle of genome defense across domains of life.

The delay in viral progression imposed by early transcriptional interference generates a window during which host adaptive responses can be engaged to preserve cellular viability. Although both +CGP3 and -CGP3 encode the same defense systems and components of the SOS pathway, activation of LexA-regulated DNA repair and defense genes was detected only in +CGP3. Canonically, SOS induction is initiated when RecA senses single-stranded DNA arising from replication anomalies, leading to LexA autoproteolysis and derepression of SOS-regulated loci, including *lexA* itself[64,65]. However, we did not detect further degradation of the LexA peptides after RecA-induced cleavage, nor derepression of *lexA* transcripts. Instead, *lexA* expression was modestly

reduced. These observations suggest that activation of LexA-regulated genes in +CGP3 may occur in a temporally restricted manner or through partially non-canonical mechanisms[66]. It is also possible that the peak of LexA proteolysis preceded the earliest sampled time point. Nevertheless, induction of SOS-associated genes was consistently supported by transcriptomic and proteomic analyses, further corroborated by microscopy revealing an elongated, division-suppressed phenotype[67]. Together, these observations indicate that the CgpS-mediated delay in phage progression enables activation of coordinated stress and DNA repair pathways that contribute to cellular resilience during infection. Recent studies have similarly shown that phage infection, even in the absence of successful lysis, can trigger the bacterial SOS response[68], and that several phage defense systems are mechanistically linked to DNA repair processes[69]. These findings further support a close functional interplay between SOS signaling and antiviral defense pathways and suggest that cooperation between multiple defense mechanisms may enhance the robustness of bacterial immunity against phage attack[70].

The capacity of CgpS to block phage infection raises broader questions regarding the functional diversification of Lsr2 proteins. In *Mycobacterium* and *Streptomyces*, Lsr2 homologues have been primarily characterized as regulators of virulence[28,71], secondary metabolism[30], and chromosome organization[22,31], and have even been reported to facilitate productive infection of certain mycobacteriophages[45]. Our phylogenetic analysis revealed that corynebacterial Lsr2 proteins (including CgpS) are distant from other ones supporting a functional diversification of the Lsr2 protein family.

CgpS is encoded within CGP3, which we suggested in previous work to be a cryptic prophage[27,72,73]. Our comparative analysis suggests now that CGP3 is a putative ICE (as it encodes Mob and T4CP proteins), which is defective in self-transmission (as the T4CP seems to be incomplete). The rapid loss of T4CP functions has been described for conjugative plasmids that have decayed into mobilizable ones[74]. Regardless of whether CGP3 is a defective prophage or an ICE, we show here that CgpS and its corynebacterial homologs are found in distinct, distantly related (wGRR < 0.05) mobile elements, a putative ICE in *C. oculi*, and a plasmid of *C. comes*. They encode Mob proteins that facilitates conjugative transfer[74]. We therefore suggest that Lsr2 proteins are frequently horizontally transferred in corynebacteria, due to their adaptive functions and may experience distinct evolutionary pressures. Furthermore, mobile genetic elements must tightly regulate their gene expression to minimize fitness costs, as described for H-NS-like proteins in 'stealth plasmids'[75]. In this context, the presence of a dedicated xenogeneic silencer encoded by the element itself may facilitate stable maintenance within the host.

In addition to Mob proteins, we identified RM systems within *cgpS*/*lsr2*-associated regions. RM systems are among the most prevalent defense modules encoded[76] and are known to influence the evolutionary trajectories of mobile elements by limiting horizontal gene transfer and phage

infection[77]. Their co-localization with Lsr2-like proteins suggests a coordinated contribution to multilayered defense and persistence strategies[78].

Elucidating antiviral strategies in Actinomycetota is particularly relevant given their ecological dominance, metabolic diversity[79], medical relevance and expanding use in biotechnology[80]. The presence of CgpS and its homologs within putative ICEs and plasmids further emphasizes the contribution of mobile genetic elements to host defense architecture. Notably, approximately 34% of chromosomal mobile elements encode complete defense systems[76], underscoring their role in the accumulation and dissemination of antiviral mechanisms. Collectively, our results further supports that mobile elements may therefore serve not only as vectors of horizontal gene transfer but also as reservoirs of modular defense traits that contribute to the pan-genomic immune repertoire of bacterial populations[81].

Methods:

Bacterial strains and growth conditions

All bacterial strains and bacteriophages used in this study are listed in Supplementary Table 1. *Escherichia coli* DH5α cells used for plasmid recombination, amplification, and storage were grown in Lysogeny Broth (LB) medium (10 g L^{-1} tryptone, 5 g L^{-1} yeast extract, 10 g L^{-1} NaCl) at 37 °C. When required, kanamycin was added at a final concentration of 50 µg mL^{-1}.

Corynebacterium glutamicum strains were cultivated in brain heart infusion (BHI) complex medium (37 g L^{-1} BHI; Difco, BD, Heidelberg, Germany). Liquid cultures were inoculated from single colonies obtained from fresh 1.5% (w/v) BHI agar plates and incubated for up to 24 h at 30 °C. Kanamycin was added when required at a final concentration of 25 µg mL^{-1}.

Pre-cultures were grown in 1 mL medium in 2.2 mL square V-bottom 96-deep-well plates (VWR, Radnor, PA, USA) sealed with breathable rayon film (VWR) and incubated at 30 °C and 900 rpm in a Microtron incubator shaker (Infors, Bottmingen, Switzerland). For larger cultures, cells were grown either in 5 mL medium in culture tubes at 170 rpm or in 20 mL medium in 50 mL baffled glass flasks with metal caps at 120 rpm and 30 °C.

For double-agar overlay assays, *C. glutamicum* precultures grown in LB medium were used to inoculate LB soft agar (0.4% agar) to a final OD_{600} of 0.3. The mixture was poured onto LB agar plates and allowed to solidify. Tenfold serial dilutions of phage lysates prepared in SM buffer (50 mM Tris–HCl, 100 mM NaCl, 8 mM $MgSO_4$, pH 7.5) were spotted onto the surface of the bacterial lawn. Plates were incubated at 30 °C for 18–24 h before plaque formation was assessed.

Microtiter cultivation for monitoring growth, infection dynamics, and fluorescence in reporter assays

Growth and infection assays were primarily monitored using the Growth Profiler 960 (EnzyScreen, Netherlands). Images of the transparent plate bottom were acquired during incubation and analyzed using GP960Viewer software (v1.1.1.0). Growth curves were calculated based on the Green Value signal, which quantifies the intensity of green pixels within a defined area of each well image.

Infection assays requiring fluorescence measurements were performed using a BioLector I® microtiter cultivation system (Beckman Coulter, Brea, CA, USA). Biomass accumulation was monitored as backscattered light intensity at 620 nm (gain factor 30). Venus fluorescence was measured using an excitation wavelength of 508 nm and emission wavelength of 532 nm (gain factor 60). Crimson fluorescence was detected at an excitation wavelength of 610 nm and emission

wavelength of 650 nm (gain factor 100). Specific fluorescence (arbitrary units, a.u.) was calculated by normalizing reporter fluorescence signals to backscatter values at each time point[82].

Infection assays were performed in BHI medium with an initial OD_{600} of 0.3 at 30 °C. Cultures were grown in volumes of 300 µL or 2 mL in the Growth Profiler system (96-well and 24-well, square white plates; 250 rpm; 85% humidity) and 750 µL in the BioLector system (48-well Flower plate; 1200 rpm; 85% humidity).

Data visualization and statistical analyses were performed using GraphPad Prism v8.0 (GraphPad Software, La Jolla, CA, USA). Graphs represent mean values with standard deviations, and statistical significance was determined using two-tailed unpaired t-tests. If not stated otherwise, n = 3.

Isolation of phage JeanGrey

Water was collected from the river Marne in France (48.881111 N, 2.705943 E). The sample was first passed through a 0.22-µm filter and then supplemented with LB (5 g/L NaCl; 5 g/L yeast extract; 10 g/L tryptone), 1 mM $CaCl_2$, and *C. glutamicum* strain MB001. After incubation for 24 h at 30 °C, the filtered supernatant produced plaques when plated in the double agar layer in the presence of MB001 and incubated for 24 h at 30 °C. The phage was further purified through three rounds of plaque picking and plating with strain MB001.

Negative-stain TEM

JeanGrey phages were collected after flooding highly confluent double-agar overlay plates with phage buffer (10 mM Tris-HCl pH 7.5; 10 mM $MgSO_4$; 1 mM $CaCl_2$; 68 mM NaCl) for 24 hours at 4 °C and subsequent passage through a 0.22-µm filter. Phages were stained with 2% wt/vol uranyl acetate and observed with a Tecnai Spirit microscope operated at 120 kV (TFS) and equipped with a Rio9 camera (Ametek/Gatan). The magnification used was 15,000× with a pixel size of 0.44 nm at the level of the specimen.

Preparation of phage lysates and purified stocks

Phage lysates were prepared using *C. glutamicum* -CGP3 as the propagation host. A 5 mL overnight culture was used to prepare double-agar overlay plates as described above, with the modification that phages were added to the bacterial soft agar mixture to a final concentration of approximately 10^5 PFU mL^{-1}. Plates were incubated at 30 °C for 24 h.

To recover phages, 5 mL SM buffer (50 mM Tris–HCl, 100 mM NaCl, 8 mM $MgSO_4$, pH 7.5) was added to each plate, and the overlays were incubated on a rocking platform for 3 h to release phage particles. The soft agar mixture was collected and centrifuged at 5,000 × g and 4 °C for 20 min to remove cellular debris. The supernatant was sterile filtered (0.2 µm) and subjected to ultracentrifugation at 37,000 × g and 4 °C for 90 min to pellet phage particles.

The resulting pellet was resuspended in 1 mL TM buffer (50 mM Tris–HCl, 10 mM $MgCl_2$, pH 7.5) and layered onto a 0–45% sucrose gradient prepared in TM buffer. Gradients were centrifuged at 28,000 rpm and 4 °C for 20 min. The visible phage band was collected using a syringe and transferred to a fresh ultracentrifugation tube containing 4 mL SM buffer, followed by a second centrifugation at 28,000 rpm and 4 °C for 90 min. The purified phage pellet was resuspended in SM buffer (pH 7.5) to the desired final volume (maximum 5 mL). For phage staining experiments, SM buffer at pH 8.5 was used instead. Phage titers were determined by double-agar overlay assays.

Phages-capsid staining with Alexa Fluor™ 488 NHS-Ester Stain

Sucrose-purified phage particles in SM buffer (pH 8.5; 500 µL) were mixed with 5 µL Alexa Fluor 647 succinimidyl ester (Thermo Fisher Scientific; 1 mg mL^{-1} in DMSO) and incubated for 1 h at 24 °C with gentle rotation. To precipitate labeled phage particles, NaCl was added to a final concentration of 1 M followed by PEG 8000 to a final concentration of 10% (w/v), and the mixture was incubated with gentle mixing for at least 30 min at 24 °C. The suspension was centrifuged at 13,000 × g for 10 min, and the pellet was resuspended in 500 µL SM buffer (pH 7.5). After a second centrifugation at 13,000 × g for 10 min, the supernatant containing labeled phage particles was collected.

Unbound dye was removed using Illustra NAP-5 desalting columns (GE Healthcare). Columns were equilibrated with 10 mL SM buffer before loading 500 µL of the labeled phage suspension. Eluted fractions (~50 µL per drop) were collected in PCR tubes and analyzed for phage titer by tenfold serial dilution using double agar overlay assays.

Fluorescence labeling was verified by mixing 1 µL of each fraction with 5 µL of *C. glutamicum* cells (OD_{600} = 0.2) and imaging adsorption events by fluorescence microscopy. Images were acquired using an Axio Imager M2 microscope (Zeiss, Oberkochen, Germany) equipped with an EC Plan-Neofluar 100×/1.3 Oil Ph3 objective and an AxioCam MRm camera (exposure time 1,040 ms, TexasRed filter: Excitation, 560/40 nm; dichroic, 595; Emission, 630/60 nm). Fractions containing fluorescently labeled phages were pooled and stored at 4 °C in the dark.

Construction of CGP3 deletion mutants

Deletion constructs were generated using the suicide vector pK19*mobsacB*[83]. Homology arms flanking the target regions were amplified by PCR using Q5® High-Fidelity 2× Master Mix (New England Biolabs, Frankfurt, Germany). PCR fragments were designed with overlapping sequences to the vector backbone and the corresponding homologous flank. The pK19*mobsacB* backbone was linearized by restriction digestion with *EcoR*I and *BamH*I.

Fragments were assembled into the linearized vector using Gibson assembly and transformed into *E. coli* DH5α by heat shock. Plasmids were verified by Sanger sequencing and subsequently introduced into *Corynebacterium glutamicum* by electroporation (Bio-Rad; 2.5 kV, 25 µF and 200 Ω). Homologous recombination events were selected using kanamycin resistance, and double-crossover recombinants were obtained by counter-selection on sucrose-containing plates. Correct genomic deletions were verified by colony PCR and sequencing.

Construction of overexpression plasmids

Overexpression constructs for *cgpS* were generated using plasmid pAN6[84], which contains a *Ptac*-controlled expression cassette with a *lacI* repressor and a C-terminal Strep-tag sequence. Target genes were amplified by PCR and assembled into the vector backbone using Gibson assembly. Expression of recombinant proteins was induced by addition of IPTG (100 µM). The C-terminal Strep-tag enabled purification of recombinant proteins and facilitated protein expression in both *E. coli* and *C. glutamicum*.

Reporter constructs and fluorescent fusion proteins

Reporter plasmids and fluorescent fusion constructs were generated using vector pJC1[85]. Promoter regions or genes of interest were amplified by PCR and assembled into the plasmid backbone by Gibson assembly. Promoter–reporter constructs were generated by cloning promoter fragments (including 30 bp of the following gene and a STOP codon) upstream of the fluorescent reporter gene *mVenus*. For localization experiments, *cgpS* was fused to *mVenus* to generate fluorescently tagged proteins.

All bacterial strains and plasmids (including the detailed information) generated in this study are listed in Supplementary Tables 1 and 2, respectively. Oligonucleotides used for cloning and sequencing are listed in Supplementary Table 4. All plasmid construction steps were performed in *Escherichia coli* DH5α.

Characterization of bacteriophage infection dynamics

Phage adsorption and intracellular phage DNA accumulation were quantified comparing *C. glutamicum* +CGP3 and-CGP3 strains. Overnight cultures grown to stationary phase were used to inoculate 20 mL BHI medium to an initial OD_{600} of 0.3 and incubated for 30 min at 30°C with shaking at 110 rpm to allow metabolic reactivation. Phages were then added at a

multiplicity of infection (MOI) of 0.4, and cultures were incubated under the same conditions for up to 6 h.

Samples were collected every 20 min during the first hour, every 30 min for the subsequent 2-3 h, and hourly thereafter. To determine free phage titers and adsorption dynamics, 10 µL samples were used for double agar overlay assays. For intracellular phage DNA quantification, 500 µL culture samples were harvested and washed twice with cold 1× PBS to remove extracellular phages. Cells were disrupted twice for 30 s at 6,500 rpm using a Precellys cell disruptor (Bertin Technologies). Lysates were centrifuged, and DNA present in the supernatant was used for downstream quantification.

Phage DNA levels were quantified by qPCR using Luna® Universal qPCR Master Mix (New England Biolabs, Ipswich, MA, USA). Reactions contained 50 ng total DNA and were performed on a qTOWER 2.2 system (Analytik Jena, Jena, Germany) according to the manufacturer's instructions. Phage DNA was detected using primers B458/B459, whereas host genomic DNA was quantified using primers B456/B457 targeting the *ddh* reference gene. qPCR reactions were performed with three biological replicates and two technical replicates per sample. Standards were generated using a dilution series of purified PCR products together with a no-template control to define the limit of detection for subsequent calculations. Relative phage DNA abundance was calculated using the comparative analysis function in qPCRsoft 3.1 (Analytik Jena), expressing phage DNA levels relative to host genomic DNA.

Reverse transcription quantitative PCR (RT-qPCR)

To quantify differences in *cgpS* expression between the wild-type strain, the +CGP3 strain, and the -CGP3 strain carrying a re-integrated copy of *cgpS* under control of its native autoregulatory promoter, transcript levels were measured by reverse transcription quantitative PCR (RT-qPCR). RT-qPCR reactions were performed using the Luna® One-Step RT–qPCR Kit (New England Biolabs, Frankfurt am Main, Germany) according to the manufacturer's instructions. Reactions were carried out on a qTOWER system (Analytik Jena, Jena, Germany) using 25 ng μL^{-1} total RNA as input.

cgpS transcript levels were quantified using primers listed in Supplementary Table 4. Expression values were normalized to the *ddh* gene of *C. glutamicum* ATCC 13032, which served as the reference gene. Data were analyzed using qPCRsoft 3.1 (Analytik Jena, Jena, Germany), and relative transcript levels were calculated using the comparative CT ($2^{-\Delta\Delta CT)}$ method described by Livak and Schmittgen[86].

RNA sequencing and transcriptome analysis

Single colonies of each tested strain were grown overnight in 5 mL BHI medium. Main cultures were inoculated to an initial OD_{600} of 0.3 in 200 mL BHI medium and incubated for 30 min at 30 °C to allow recovery from stationary phase and metabolic reactivation. Purified JeanGrey phage stocks were then added to a final multiplicity of infection (MOI) of 1.

For-CGP3 samples, cultures were harvested at 15- and 60-min post infection. For +CGP3 samples, cultures were harvested at 15, 30, and 60 min post infection. Uninfected +CGP3 controls were collected at the same time points (n = 2). Cells were harvested by centrifugation (15 min, 11,325 × g, 4 °C) in the presence of crushed ice. Cell pellets were snap-frozen in liquid nitrogen and stored at −80 °C until RNA extraction.

Total RNA was isolated using the Monarch Total RNA Miniprep Kit (New England Biolabs, Ipswich, MA, USA) according to the manufacturer's instructions. rRNA depletion, library preparation, quality control, and paired-end sequencing (2 × 150 bp) on an Illumina NovaSeq platform with approximately 10 million read pairs per sample were performed by Genewiz (Leipzig, Germany).

Raw reads were further quality controlled, adapter-trimmed, and filtered using CLC Genomics Workbench v24 (Qiagen, Hilden, Germany). Reads containing low-quality bases (error probability > 0.05) or ambiguous nucleotides were removed. Reference genomes were generated by modifying the *C. glutamicum* ATCC 13032 genome sequence (NCBI accession BX927147) to reflect the +CGP3 and-CGP3 strain backgrounds and combining these with the JeanGrey phage genome sequence (Genbank accession PZ176366).

Transcript abundances were calculated as transcripts per million (TPM) using the RNA-Seq Analysis tool in CLC Genomics Workbench (parameters: mismatch cost 2; insertion cost 3; deletion cost 3; length fraction 0.9; similarity fraction 0.9; maximum hits per read 10; strand specificity both; library type bulk). Differential gene expression between infected and non-infected samples was determined using the "Differential Expression in Two Groups" function in CLC. Genes were considered significantly differentially expressed when they met the following criteria: FDR-adjusted P value < 0.05, maximum group mean transcript abundance > 10, and $|\log_2$ fold change$|$ > 1. P values were calculated using a generalized linear model assuming a negative binomial distribution and corrected for multiple testing using the Benjamini–Hochberg false discovery rate method[87]. A summary of sample information, TPM values and differential expression results is provided in Supplementary Table 7.

Protein Isolation for proteomic analysis

Overnight cultures (n = 3 biological replicates) grown to stationary phase were used to inoculate 20 mL BHI medium to an initial OD_{600} of 0.6. Cultures were incubated for 30 min at 30°C with shaking at 110 rpm to allow metabolic reactivation. An initial sample (t_0) was collected prior to phage infection. For protein isolation, 2 mL culture aliquots were harvested by centrifugation at 13,000 rpm and 4°C. Supernatants were carefully removed, and cell pellets were immediately frozen in liquid nitrogen.

Phages were subsequently added at a multiplicity of infection (MOI) of 1, and cultures were incubated under the same conditions for 1 h. Samples were collected at 15-, 30-, and 60-min post infection following the same harvesting procedure.

Cell pellets were resuspended in 300 µL proteomics lysis buffer (100 mM ammonium bicarbonate (ABC), 1% sodium lauryl sulfate (SLS), 1 mg/mL lysozyme) and incubated for 5 min at room temperature. The cell suspension was heat-treated at 95 °C for 10 min. Suspensions were then transferred to 2 mL FastPrep tubes (MP Biomedicals) containing 0.1 g of 0.1 mm glass beads (Scientific Industries Inc.) and cells were lysed by two cycles of bead beating using a FastPrep-25 5G (MP Biomedicals) at 6.0 m s^{-1} for 60 s.

The lysate was transferred to a new tube, and 600 µL of 100 mM ABC containing 10 U benzonase was added to each sample. Samples were mixed briefly by vortexing and incubated at 30 °C with shaking (350 rpm) for 1 h. Proteins were reduced by addition of tris(2-carboxyethyl)phosphine (TCEP) to a final concentration of 2 mM (40 °C, 10 min) and alkylated with iodoacetamide added to a final concentration of 4 mM (30 min, room temperature, in the dark).

Samples were centrifuged at 10,000 × g for 10 min at 4 °C and the supernatant was transferred to a fresh tube. Proteins were precipitated by addition of five volumes of ice-cold acetone and incubation at −20 °C for 4 h. Proteins were collected by centrifugation at 10,000 × g for 10 min at 4 °C. The supernatant was discarded, and pellets were washed with 500 µL cold methanol, which was then removed by repeated precipitation.

Dry protein pellets were resuspended in 200 µL of 100 mM ABC containing 0.1% SLS. Protein concentrations were determined using a Pierce™ BCA assay (Thermo Fisher Scientific). For digestion, 20 µg protein per sample was digested with 0.5 µg trypsin overnight at 30 °C. Following digestion, SLS was precipitated by addition of TFA to a final concentration of 1% (v/v), and the supernatant was collected. The supernatant was desalted for mass spectrometric analysis using C18 solid-phase columns (Chromabond C18 spin columns; Macherey-Nagel, Düren, Germany). The desalted peptides were used for LC–MS analysis.

LC-MS/MS Analysis

Samples were measured using the Vanquish Neo UHPLC System (ThermoFisher Scientific, Waltham, MA USA) coupled to an Orbitrap Exploris 480 mass spectrometer with a FAIMSpro interface (ThermoFisher Scientific, Waltham, MA USA). Peptides were separated on an µPAC NEO HPLC column (COL-NANO050NEOB, ThermoFisher Scientific, Waltham, MA USA) operated at 50°C, using 38-minute gradient (250 nl/min, 10% Buffer B at minute 4, 22% at minute 23, 45% at minute 31, 95% at min 34 until the end of the gradient). Eluting peptides were injected into the mass spectrometer with an EASY-Spray nano Flow Emitter (ES993, ThermoFisher Scientific, Waltham, MA USA) at a static voltage of 2000 V, with a carrier gas flow of 3.6 L/min and an ion transfer tube temperature of 225 °C. FAIMS was operated at standard resolution and one compensation voltage of -45. MS1 scans were acquired at 120,000 resolution across a mass range of 400–1000 m/z, automatic maximum injection time, normalized AGC target of 3e6, RF Lens at 40%, using profile mode. Data independent MS/MS scans were acquired with an HRMS1 DIA method[88] at 60,000 resolution, with an isolation window of 6 m/z (with loop N, 33 scans each), first mass at 200 m/z, HCD fragmentation at 30% normalized collision energy, AGC target of 1e6, and automatic maximum injection time. Raw data were analyzed using DIA-NN[89] (v2.0.2, academia), searching against the custom databases comprising protein FASTA sequences of *C. glutamicum* ATCC 13032 (Genbank accession BX927147) and bacteriophage JeanGrey (Genbank accession PZ176366), concatenated into a single reference database. Search parameters included a step for FASTA digest for library-free search with deep learning-based spectra, RTs and Ims prediction, using Trypsin/P as protease, allowing for two missed cleavages and one variable modification. N-terminal methionine excision, cysteine carbamidomethylation, methionine oxidation, and N-terminal acetylation were included in the library, with peptide, precursor and fragment ranges set to default (6-36 amino acids, 1-4 charge states, 300-1800 precursor m/z range, 200-1800 fragment m/z range). Main search was performed with constructed library using MS1 quantification and QuantUMS[90], at 1% precursor FDR with peptidoform scoring and FASTA protein names proteotypicity and otherwise default settings.

In vitro protein-DNA interaction with bandshift assays (EMSAs)

For in vitro protein–DNA interaction assays, CgpS carrying a C-terminal Strep-tag® was heterologously expressed in *Escherichia coli* BL21 (DE3). Cells were grown at 37 °C to an OD_{600} of 0.4 and protein expression was induced with 100 µM IPTG. Cultures were then incubated overnight at 18 °C. Cells were harvested by centrifugation (5,300 × g, 10 min, 4 °C) and resuspended in buffer B (250 mM NaCl, 50 mM Tris–HCl, pH 7.5). Cells were disrupted by a single passage through a Multi Shot Cell Disruptor (I&L Biosystems, Germany). Cellular debris was removed by centrifugation (5,300 × g, 20 min, 4 °C), followed by ultracentrifugation (229,000 × g, 60 min, 4 °C).

The clarified lysate was applied to a 1 mL Strep-Tactin® Sepharose® column (IBA, Göttingen, Germany) equilibrated with buffer B. After washing with 10 mL buffer B, CgpS was eluted with 5 mL buffer B supplemented with 1 mM d-desthiobiotin (Sigma-Aldrich).

EMSAs were performed using purified CgpS and selected phage-derived DNA fragments (Supplementary Table 6). DNA fragments (~200 bp) were amplified by PCR using primers listed in Supplementary Table 4 and purified using a PCR Clean-up Kit (Macherey-Nagel, Düren, Germany). The promoter region of *gntK* served as a negative control, whereas the *cgpS* promoter region was used as a positive control. For each reaction, 90 ng DNA were incubated with increasing concentrations of purified CgpS for 30 min in EMSA buffer (250 mM Tris–HCl pH 7.5, 25 mM $MgCl_2$, 200 mM KCl, 25% (v/v) glycerol).

Samples were separated on native 10% polyacrylamide gels prepared in 1× TBE buffer (89 mM Tris base, 89 mM boric acid, 2 mM Na_2EDTA). Gels were run in 1× TBE and stained with ethidium bromide. DNA bands were visualized using a UV transilluminator.

Chromatin affinity purification sequencing (ChAP–seq) sample preparation

DNA–protein complexes were isolated using a protocol adapted from previous studies[38]. The strain *C. glutamicum* ATCC 13032(+CGP3)::*cgpS*–CStrep was cultivated in biological triplicates as described in the section “Bacterial strains and growth conditions”. After 30 min of growth at 30 °C with shaking (110 rpm), cultures were infected with purified JeanGrey phage to a final multiplicity of infection (MOI) of 1. Cells were harvested 15 min post infection by centrifugation (5,000 × g, 10 min, 4 °C).

For plasmid-based ChAP–seq experiments, *C. glutamicum* ATCC 13032(+CGP3)::*cgpS*–CStrep cells were transformed with plasmids carrying selected phage promoter regions fused to *venus*. The plasmids used in this study are listed in Supplementary Table 2. Cultures were grown for 4 h prior to harvesting. All subsequent purification steps were performed identically for both experimental approaches.

Cell pellets were washed once with CGXII base solution without MOPS (1 g L^{-1} K_2HPO_4, 1 g L^{-1} KH_2PO_4, 5 g L^{-1} urea, pH 7.0), and protein–DNA complexes were purified following the protocol described by Krüger et al.[38]. For purification of DNA bound to CgpS, the Strep-tag affinity protocol was used. Cells were treated in buffer A (100 mM Tris–HCl, pH 8.0; without EDTA to avoid chelation of divalent ions). Strep-tagged CgpS and associated DNA were purified using Strep-Tactin column material (IBA Lifesciences, Göttingen, Germany) according to the manufacturer’s gravity-flow protocol. Columns were washed with buffer W (100 mM Tris–HCl, 150 mM NaCl, pH 8.0), and protein–DNA complexes were eluted with buffer E (100 mM Tris–HCl, 150 mM NaCl, 15 mM D-biotin, pH 8.0).

Input DNA controls were prepared from lysed cell cultures without affinity purification. Purified DNA samples were processed following the protocol described in Krüger et al.[38] and stored at −20°C until further analysis.

ChAP-Seq – Sequencing and DNA Enrichment Analysis

DNA fragments obtained from chromatin affinity purification were used for library preparation using the TruSeq DNA PCR-Free Sample Preparation Kit (Illumina, Chesterford, UK) according to the manufacturer's instructions, omitting the DNA size-selection step. Libraries were quantified using the KAPA Library Quantification Kit (Peqlab, Bonn, Germany) and normalized prior to pooling.

Pooled libraries were sequenced on an Illumina MiSeq platform using paired-end sequencing (2 × 150 bp). Base calling and initial data processing were performed using the Illumina instrument software, generating FASTQ files for downstream analysis.

Subsequent data processing was performed following a workflow adapted from Keppel et al.[91] To reduce PCR amplification artifacts, sequencing reads were collapsed for each sample prior to mapping. Processed reads were mapped to a modified *C. glutamicum* ATCC 13032 reference genome (NCBI accession BX927147) reflecting the +CGP3 and −CGP3 strain backgrounds. For infection experiments, the JeanGrey phage genome sequence was included in the reference assembly, whereas plasmid sequences were included for plasmid-based ChAP–seq experiments.

Read mapping and peak detection were performed as described in the methods of Krüger et al. (2025)[38]. Enrichment of selected regions identified by peak analysis was validated by qPCR comparing affinity-purified DNA to input DNA controls. qPCR procedures were performed as described in the section "Characterization of bacteriophage infection dynamics".

Fluorescence single-cell microfluidic microscopy

Single-cell analyses were performed using an in-house developed microfluidic platform[92-94]. *C. glutamicum* +CGP3 cells carrying the re-localization plasmid encoding for a CgpS–mVenus fusion protein were cultivated in microfluidic chambers measuring 60 × 60 µm with a chamber height of 1.02–1.04 µm.

Time-lapse imaging was performed using phase-contrast and fluorescence microscopy at 5 min intervals. Fluorescence signals were recorded using a Texas Red filter set (excitation 560/40 nm, dichroic 595 nm, emission 630/60 nm) and a YFP filter set (excitation 520/530 nm, dichroic 630 nm, emission 540/20 nm).

826 Medium was continuously supplied to the chambers to maintain stable environmental conditions.
827 Either BHI medium (control) or BHI supplemented with phages (final concentration 10^7 PFU mL^{-1})
828 was infused at a flow rate of 300 nL min^{-1} using a high-precision syringe pump (neMESYS, Cetoni
829 GmbH, Korbussen, Germany). The cultivation temperature was maintained at 30°C using a
830 temperature control unit (PeCon GmbH, Erbach, Germany). Cells were cultivated and monitored
831 for 3 h.

832 Image processing, including preparation of image cutouts and adjustment of lookup tables (LUTs),
833 was performed using NIS-Elements BR version 5.30.03 (64-bit).

834

835 ## Microscopy of the infection cycle with agarose pads

836 *C. glutamicum* +CGP3 and -CGP3 cells were cultivated overnight in BHI medium es described
837 before. The following day, cultures were diluted in fresh medium and grown for 30 min to resume
838 active growth. Phages were then added at a multiplicity of infection (MOI) of 1 and incubated for
839 25 min at 30°C with shaking at 110 rpm to allow adsorption. Cells were subsequently collected by
840 centrifugation and resuspended in 1/5 fresh BHI medium.

841 For microscopy, 3 µL of the culture were spotted onto a 2% BHI agarose pad mounted on a glass
842 coverslip. Time-lapse phase-contrast imaging was performed using a Leica Mica confocal
843 microscope equipped with a complementary metal–oxide–semiconductor (CMOS) camera. Images
844 were acquired with a ×63 water-immersion objective at 5-min intervals for 240 min in a
845 temperature-controlled chamber maintained at 30°C with humidity control.

846 Image processing was performed using Leica LAS X software v.6.2.1. Further image cropping and
847 time-lapse video generation were carried out using ImageJ v.1.54g.

848

849 ## Collecting bacterial, phage, and Lsr2 sequences

850 Bacterial and phage genomes used in this work were retrieved from GenBank[95], RefSeq[96], and
851 INPHARED[46] (accession IDs and database sources are listed in Supplementary Table 8). In total,
852 34076 phage sequences were downloaded from INPHARED (database version 14Apr2025). From
853 RefSeq and GenBank, we retrieved 174 coryne- and 5 mycobacterial sequences. We screened all
854 genomes for genes encoding Lsr2 by comparing the protein sequences to Pfam[97] profiles
855 (PF11774: dimerization and PF23359: DNA-binding) of Lsr2 with hmmer v3.4[98]. All protein
856 sequences covering at least 50% of the profiles and domain i-evalues =< 0.001 were kept and
857 annotated as Lsr2 if matched both profiles. In total, this led to the annotation of 540 complete Lsr2
858 protein sequences (Supplementary Table 8).

Phylogenetic protein tree of Lsr2

We aligned all Lsr2 sequences with mafft[99](default) and used the global alignment (276 positions and 261 distinct patterns) to compute a maximum-likelihood tree with IQ-TREE2[100]. We computed 1000 ultrafast bootstraps (adding '-B 1000') to assess robustness. Q.pfam+I+G4 was selected (with '-m TEST') as the best evolutionary model, representing a general substitution matrix (trained on the Pfam database), with important invariable sites and different rates. Processing and visualization were done in R using the packages ape[101], phytools[102], and ggtree[103].

Comparative analysis and annotation of Lsr2 regions

We examine the genomic content in proximity to the Lsr2 genes, we extracted regions having up to 50 genes up and downstream of Lsr2 from all corynebacterial and mycobacterial genomes. If *lsr2* was encoded on sequences with fewer neighboring genes, such as plasmids or short contigs from draft genomes, the extraction resulted in regions having less than 100 genes. We annotated these Lsr2 regions using geNomad v. 1.11.0 with database version 1.8.0 (in default mode)[57], DefenseFinder 2.0.1 (default)[42], and profiles of conjSCAN[47]. Information on the regions (position, gene IDs, annotations) are summarized in Supplementary Table 9. To assess genetic relationships between the regions, we computed the weighted gene repertoire relatedness (wGRR), as reported elsewhere[104].

We used gggenomes (https://thackl.r-universe.dev/articles/gggenomes/gggenomes.html) to visualize regions and annotations.

Data availability:

The genome sequence of bacteriophage Jean Grey has been deposited in GenBank under accession number PZ176366. The RNA-Seq data under infection conditions were deposited in the European Nucleotide Archive (ENA) at EMBL-EBI (https://www.ebi.ac.uk/ena/browser/home) under accession number PRJEB109319. The Plasmid-based ChAP-Seq data were deposited in the European Nucleotide Archive (ENA) at EMBL-EBI (https://www.ebi.ac.uk/ena/browser/home) under accession number PRJEB108477. The ChAP-Seq under infection conditions data were deposited in the European Nucleotide Archive (ENA) at EMBL-EBI (https://www.ebi.ac.uk/ena/browser/home) under accession number PRJEB109751. The mass spectrometry proteomics data have been deposited to the ProteomeXchange Consortium via the PRIDE[105] partner repository with the dataset identifier PXD075760.

Funding:

We thank the Jürgen Manchot Stiftung and the Jürgen Manchot Graduate School “Molecules of Infection”, MOI V, for financial support for B.B.R.. We thank the Deutsche Forschungsgemeinschaft (SPP 2330 “New concepts in prokaryotic virus-host interaction”, project 464434020) for financial support to J.F.. K.K. is supported by a Novo Nordisk Foundation Young Investigator Award (grant no. NNF16OC0020670) and a postdoctoral fellowship grant from the Independent Research Fund Denmark (grant no. 4257-00010B). N.P. is supported by EMBO Postdoctoral Fellowship (ALTF 765-2025). S.J.J.B is supported by a grant from the European Research Council (ERC) CoG under the European Union’s Horizon 2020 research and innovation program (grant agreement no. 101003229). K.L.M. is the Canada Research Chair in Bacteriophage Biology and Therapeutics (CRC-2023-00010) and the lab is supported by the Canadian Institutes of Health Research (PJT-203903). Seed funding was provided by the “Appel à projet pour la pédagogie” from the Ecole Universitaire de Premier Cycle of University Paris-Saclay to O.R.. The present work has benefited from the platform of Cryo-EM of I2BC supported by IBiSA and by French Infrastructure for Integrated Structural Biology (FRISBI) ANR-10-INBS-05. Furthermore, this work was supported in part by the French junior professor chair ANR grant for EP (ANR-22-CPJ1-0041-01).

Acknowledgments:

We thank the students who participated the characterization of phage JeanGrey through the Phage Discovery and Phage DNA Explorer programs of the University Paris-Saclay, ie Elsa Chaouat, Océane Hill, Kenza Bahraoui, Tatiana Brun, and Ashvini Srimoorthy. We acknowledge the High throughput sequencing facility of l2BC for its sequencing and bioinformatics expertise.

We are grateful to the INRAE MIGALE bioinformatics facility (MIGALE, INRAE, 2020. Migale bioinformatics Facility, doi: 10.15454/1.5572390655343293E12) for providing computing and storage resources.

We thank Dr. Eva Davoudi for the conceptualization of the CGP3 deletion library and generation of cloning and sequencing primers.

Literature:

1 Soucy, S. M., Huang, J. & Gogarten, J. P. Horizontal gene transfer: building the web of life. *Nat Rev Genet* **16**, 472–482 (2015). https://doi.org/10.1038/nrg3962

2 Daubin, V. & Ochman, H. Start-up entities in the origin of new genes. *Curr Opin Genet Dev* **14**, 616–619 (2004). https://doi.org/10.1016/j.gde.2004.09.004

3 Toft, C. & Andersson, S. G. Evolutionary microbial genomics: insights into bacterial host adaptation. *Nat Rev Genet* **11**, 465–475 (2010). https://doi.org/10.1038/nrg2798

4 Thomas, C. M. & Nielsen, K. M. Mechanisms of, and barriers to, horizontal gene transfer between bacteria. *Nat Rev Microbiol* **3**, 711–721 (2005). https://doi.org/10.1038/nrmicro1234

5 Hendrix, R. W. Bacteriophages: evolution of the majority. *Theor Popul Biol* **61**, 471–480 (2002). https://doi.org/10.1006/tpbi.2002.1590

6 Baltrus, D. A. Exploring the costs of horizontal gene transfer. *Trends Ecol Evol* **28**, 489–495 (2013). https://doi.org/10.1016/j.tree.2013.04.002

7 Lamberte, L. E. *et al.* Horizontally acquired AT-rich genes in Escherichia coli cause toxicity by sequestering RNA polymerase. *Nat Microbiol* **2**, 16249 (2017). https://doi.org/10.1038/nmicrobiol.2016.249

8 Hendrix, R. W., Smith, M. C., Burns, R. N., Ford, M. E. & Hatfull, G. F. Evolutionary relationships among diverse bacteriophages and prophages: all the world's a phage. *Proc Natl Acad Sci U S A* **96**, 2192–2197 (1999). https://doi.org/10.1073/pnas.96.5.2192

9 Hendrix, R. W. Evolution: the long evolutionary reach of viruses. *Curr Biol* **9**, R914–917 (1999). https://doi.org/10.1016/s0960-9822(00)80103-7

10 Hassen, B. & Hammami, S. Environmental phages: ecosystem dynamics, biotechnological applications and their limits, and future directions. *J Appl Microbiol* **136** (2025). https://doi.org/10.1093/jambio/lxaf136

11 Jaglan, A. B. *et al.* Tracking the phage trends: A comprehensive review of applications in therapy and food production. *Front Microbiol* **13**, 993990 (2022). https://doi.org/10.3389/fmicb.2022.993990

12 Strathdee, S. A., Hatfull, G. F., Mutalik, V. K. & Schooley, R. T. Phage therapy: From biological mechanisms to future directions. *Cell* **186**, 17–31 (2023). https://doi.org/10.1016/j.cell.2022.11.017

13 Seed, K. D. Battling Phages: How Bacteria Defend against Viral Attack. *PLoS Pathog* **11**, e1004847 (2015). https://doi.org/10.1371/journal.ppat.1004847

14 Gordon, B. R. *et al.* Structural basis for recognition of AT-rich DNA by unrelated xenogeneic silencing proteins. *Proc Natl Acad Sci U S A* **108**, 10690–10695 (2011). https://doi.org/10.1073/pnas.1102544108

15 Duan, B., Ding, P., Navarre, W. W., Liu, J. & Xia, B. Xenogeneic Silencing and Bacterial Genome Evolution: Mechanisms for DNA Recognition Imply Multifaceted Roles of Xenogeneic Silencers. *Mol Biol Evol* **38**, 4135–4148 (2021). https://doi.org/10.1093/molbev/msab136

16 Singh, K., Milstein, J. N. & Navarre, W. W. Xenogeneic Silencing and Its Impact on Bacterial Genomes. *Annu Rev Microbiol* **70**, 199–213 (2016). https://doi.org/10.1146/annurev-micro-102215-095301

17 Dersch, P., Schmidt, K. & Bremer, E. SYNTHESIS OF THE ESCHERICHIA-COLI K-12 NUCLEOID-ASSOCIATED DNA-BINDING PROTEIN H-NS IS SUBJECTED TO GROWTH-PHASE CONTROL AND AUTOREGULATION. *Molecular Microbiology* **8**, 875–889 (1993). https://doi.org/10.1111/j.1365-2958.1993.tb01634.x

18 Smits, W. K. & Grossman, A. D. The Transcriptional Regulator Rok Binds A plus T-Rich DNA and Is Involved in Repression of a Mobile Genetic Element in Bacillus subtilis. *Plos Genetics* **6** (2010). https://doi.org/10.1371/journal.pgen.1001207

19 Gordon, B. R., Imperial, R., Wang, L., Navarre, W. W. & Liu, J. Lsr2 of Mycobacterium represents a novel class of H-NS-like proteins. *J Bacteriol* **190**, 7052–7059 (2008). https://doi.org/10.1128/JB.00733-08

20 Sharma, V., Hardy, A., Luthe, T. & Frunzke, J. Phylogenetic Distribution of WhiB- and Lsr2-Type Regulators in Actinobacteriophage Genomes. *Microbiol Spectr* **9**, e0072721 (2021). https://doi.org/10.1128/Spectrum.00727-21

21 Kronheim, S. *et al.* Complete genomes and comparative analyses of Streptomyces phages that influence secondary metabolism and sporulation. *Sci Rep* **13**, 9820 (2023). https://doi.org/10.1038/s41598-023-36938-z

22 Gehrke, E. J. *et al.* Silencing cryptic specialized metabolism in Streptomyces by the nucleoid-associated protein Lsr2. *Elife* **8** (2019). https://doi.org/10.7554/eLife.47691

23 Kolodziej, M. *et al.* Lsr2, a nucleoid-associated protein influencing mycobacterial cell cycle. *Sci Rep* **11**, 2910 (2021). https://doi.org/10.1038/s41598-021-82295-0

24 Wiechert, J. *et al.* Deciphering the Rules Underlying Xenogeneic Silencing and Counter-Silencing of Lsr2-like Proteins Using CgpS of Corynebacterium glutamicum as a Model. *Mbio* **11** (2020). https://doi.org/10.1128/mBio.02273-19

25 Gordon, B. R. G. *et al.* Lsr2 is a nucleoid-associated protein that targets AT-rich sequences and virulence genes in Mycobacterium tuberculosis. *Proceedings of the National Academy of Sciences of the United States of America* **107**, 5154–5159 (2010). https://doi.org/10.1073/pnas.0913551107

26 Summers, E. L. *et al.* The structure of the oligomerization domain of Lsr2 from Mycobacterium tuberculosis reveals a mechanism for chromosome organization and protection. *PLoS One* **7**, e38542 (2012). https://doi.org/10.1371/journal.pone.0038542

27 Pfeifer, E. *et al.* Silencing of cryptic prophages in Corynebacterium glutamicum. *Nucleic Acids Research* **44**, 10117–10131 (2016). https://doi.org/10.1093/nar/gkw692

28 Le Moigne, V. *et al.* Lsr2 Is an Important Determinant of Intracellular Growth and Virulence in Mycobacterium abscessus. *Front Microbiol* **10**, 905 (2019). https://doi.org/10.3389/fmicb.2019.00905

29 Ling, X. *et al.* Lsr2 acts as a cyclic di-GMP receptor that promotes keto-mycolic acid synthesis and biofilm formation in mycobacteria. *Nat Commun* **15**, 695 (2024). https://doi.org/10.1038/s41467-024-44774-6

30 Cuervo, L., Malmierca, M. G. & Olano, C. An Overview of Lsr2 Repressor Effect in Streptomyces spp. Secondary Metabolism. *Microorganisms* **12** (2024). https://doi.org/10.3390/microorganisms12112317

31 Ramirez, V. *et al.* LsrL modulates Lsr2-induced chromatin structure to tune biosynthetic gene cluster regulation in Streptomyces venezuelae. *bioRxiv* (2025). https://doi.org/10.1101/2025.11.23.690019

32 Frunzke, J., Bramkamp, M., Schweitzer, J. E. & Bott, M. Population Heterogeneity in Corynebacterium glutamicum ATCC 13032 caused by prophage CGP3. *J Bacteriol* **190**, 5111–5119 (2008). https://doi.org/10.1128/JB.00310-08

33 Baumgart, M. *et al.* Construction of a prophage-free variant of Corynebacterium glutamicum ATCC 13032 for use as a platform strain for basic research and industrial biotechnology. *Appl Environ Microbiol* **79**, 6006–6015 (2013). https://doi.org/10.1128/AEM.01634-13

34 Schafer, A., Tauch, A., Droste, N., Puhler, A. & Kalinowski, J. The Corynebacterium glutamicum cglIM gene encoding a 5-cytosine methyltransferase enzyme confers a specific DNA methylation pattern in an McrBC-deficient Escherichia coli strain. *Gene* **203**, 95–101 (1997). https://doi.org/10.1016/s0378-1119(97)00519-2

35 Pfeifer, E., Hunnefeld, M., Popa, O. & Frunzke, J. Impact of Xenogeneic Silencing on Phage-Host Interactions. *Journal of Molecular Biology* **431**, 4670–4683 (2019). https://doi.org/10.1016/j.jmb.2019.02.011

36 Hunnefeld, M. *et al.* Genome Sequence of the Bacteriophage CL31 and Interaction with the Host Strain *Corynebacterium glutamicum* ATCC 13032. *Viruses* **13** (2021). https://doi.org/10.3390/v13030495

37 Rossier, O. *et al.* Genome sequence of PSonyx, a singleton bacteriophage infecting Corynebacterium glutamicum. *Microbiol Resour Announc* **13**, e0115523 (2024). https://doi.org/10.1128/mra.01155-23

38 Kruger, A., Weber, U. & Frunzke, J. Genome-Wide Analysis of DtxR and HrrA Regulons Reveals Novel Targets and a High Level of Interconnectivity Between Iron and Heme Regulatory Networks in Corynebacterium glutamicum. *Mol Microbiol* **124**, 115–130 (2025). https://doi.org/10.1111/mmi.15376

39 Chen, J. M. *et al.* Lsr2 of Mycobacterium tuberculosis is a DNA-bridging protein. *Nucleic Acids Res* **36**, 2123–2135 (2008). https://doi.org/10.1093/nar/gkm1162

40 Santoshi, M., Tare, P. & Nagaraja, V. Nucleoid-associated proteins of mycobacteria come with a distinctive flavor. *Mol Microbiol* **123**, 177–194 (2025). https://doi.org/10.1111/mmi.15287

41 Weiss, M. *et al.* The MksG nuclease is the executing part of the bacterial plasmid defense system MksBEFG. *Nucleic Acids Res* **51**, 3288–3306 (2023). https://doi.org/10.1093/nar/gkad130

42 Tesson, F. *et al.* Systematic and quantitative view of the antiviral arsenal of prokaryotes. *Nat Commun* **13**, 2561 (2022). https://doi.org/10.1038/s41467-022-30269-9

43 Little, J. W. Mechanism of specific LexA cleavage: autodigestion and the role of RecA coprotease. *Biochimie* **73**, 411–421 (1991). https://doi.org/10.1016/0300-9084(91)90108-d

44 Ogino, H., Teramoto, H., Inui, M. & Yukawa, H. DivS, a novel SOS-inducible cell-division suppressor in Corynebacterium glutamicum. *Mol Microbiol* **67**, 597–608 (2008). https://doi.org/10.1111/j.1365-2958.2007.06069.x

45 Dulberger, C. L. *et al.* Mycobacterial nucleoid-associated protein Lsr2 is required for productive mycobacteriophage infection. *Nat Microbiol* **8**, 695–710 (2023). https://doi.org/10.1038/s41564-023-01333-x

46 Cook, R. *et al.* INfrastructure for a PHAge REference Database: Identification of Large-Scale Biases in the Current Collection of Cultured Phage Genomes. *Phage (New Rochelle)* **2**, 214–223 (2021). https://doi.org/10.1089/phage.2021.0007

47 Cury, J., Abby, S. S., Doppelt-Azeroual, O., Neron, B. & Rocha, E. P. C. Identifying Conjugative Plasmids and Integrative Conjugative Elements with CONJscan. *Methods Mol Biol* **2075**, 265–283 (2020). https://doi.org/10.1007/978-1-4939-9877-7_19

48 Bernard, K. The genus corynebacterium and other medically relevant coryneform-like bacteria. *J Clin Microbiol* **50**, 3152–3158 (2012). https://doi.org/10.1128/JCM.00796-12

49 Bernard, K. A. *et al.* Corynebacterium lowii sp. nov. and Corynebacterium oculi sp. nov., derived from human clinical disease and an emended description of Corynebacterium mastitidis. *Int J Syst Evol Microbiol* **66**, 2803–2812 (2016). https://doi.org/10.1099/ijsem.0.001059

50 Funke, G., von Graevenitz, A., Clarridge, J. E., 3rd & Bernard, K. A. Clinical microbiology of coryneform bacteria. *Clin Microbiol Rev* **10**, 125–159 (1997). https://doi.org/10.1128/CMR.10.1.125

51 Gilroy, R. *et al.* Extensive microbial diversity within the chicken gut microbiome revealed by metagenomics and culture. *PeerJ* **9**, e10941 (2021). https://doi.org/10.7717/peerj.10941

52 Baer, M. K. *et al.* Corynebacterium suedekumii sp. nov and Corynebacterium breve sp. nov., isolated from raw cow's milk. *Int J Syst Evol Microbiol* **73** (2023). https://doi.org/10.1099/ijsem.0.006141

53 Hashish, E. *et al.* Mycobacterium marinum infection in fish and man: epidemiology, pathophysiology and management; a review. *Vet Q* **38**, 35–46 (2018). https://doi.org/10.1080/01652176.2018.1447171

54 Hinic, V. *et al.* Corynebacterium tuberculostearicum: a potentially misidentified and multiresistant Corynebacterium species isolated from clinical specimens. *J Clin Microbiol* **50**, 2561–2567 (2012). https://doi.org/10.1128/JCM.00386-12

55 Silva Ado, S. *et al.* Draft Genome Sequence of Corynebacterium ulcerans FRC58, Isolated from the Bronchitic Aspiration of a Patient in France. *Genome Announc* **2** (2014). https://doi.org/10.1128/genomeA.01132-13

56 Cappelli, E. A. *et al.* Expanding the Bacterial Diversity of the Female Urinary Microbiome: Description of Eight New Corynebacterium Species. *Microorganisms* **11** (2023). https://doi.org/10.3390/microorganisms11020388

57 Camargo, A. P. *et al.* Identification of mobile genetic elements with geNomad. *Nat Biotechnol* **42**, 1303–1312 (2024). https://doi.org/10.1038/s41587-023-01953-y

58 Georjon, H., Tesson, F., Shomar, H. & Bernheim, A. Genomic characterization of the antiviral arsenal of Actinobacteria. *Microbiology (Reading)* **169** (2023). https://doi.org/10.1099/mic.0.001374

59 Bouffartigues, E., Buckle, M., Badaut, C., Travers, A. & Rimsky, S. H-NS cooperative binding to high-affinity sites in a regulatory element results in transcriptional silencing. *Nat Struct Mol Biol* **14**, 441–448 (2007). https://doi.org/10.1038/nsmb1233

60 Will, W. R., Navarre, W. W. & Fang, F. C. Integrated circuits: how transcriptional silencing and counter-silencing facilitate bacterial evolution. *Current Opinion in Microbiology* **23**, 8–13 (2015). https://doi.org/10.1016/j.mib.2014.10.005

61 Wiechert, J. *et al.* CRISPR/dCas-mediated counter-silencing: reprogramming dCas proteins into antagonists of xenogeneic silencers. *mBio* **16**, e0038225 (2025). https://doi.org/10.1128/mbio.00382-25

62 Conn, K. L., Hendzel, M. J. & Schang, L. M. Core histones H2B and H4 are mobilized during infection with herpes simplex virus 1. *J Virol* **85**, 13234–13252 (2011). https://doi.org/10.1128/JVI.06038-11

63 Roberts, A. P. E. *et al.* Daxx mediated histone H3.3 deposition on HSV-1 DNA restricts genome decompaction and the progression of immediate-early transcription. *PLoS Pathog* **21**, e1012501 (2025). https://doi.org/10.1371/journal.ppat.1012501

64 Brent, R. & Ptashne, M. Mechanism of action of the lexA gene product. *Proc Natl Acad Sci U S A* **78**, 4204–4208 (1981). https://doi.org/10.1073/pnas.78.7.4204

65 Little, J. W., Mount, D. W. & Yanisch-Perron, C. R. Purified lexA protein is a repressor of the recA and lexA genes. *Proc Natl Acad Sci U S A* **78**, 4199–4203 (1981). https://doi.org/10.1073/pnas.78.7.4199

66 Sanchez-Osuna, M. *et al.* Non-canonical LexA proteins regulate the SOS response in the Bacteroidetes. *Nucleic Acids Res* **49**, 11050–11066 (2021). https://doi.org/10.1093/nar/gkab773

67 Jochmann, N. *et al.* Genetic makeup of the Corynebacterium glutamicum LexA regulon deduced from comparative transcriptomics and in vitro DNA band shift assays. *Microbiology (Reading)* **155**, 1459–1477 (2009). https://doi.org/10.1099/mic.0.025841-0

68 Pons, B. J. *et al.* Phage provoke growth delays and SOS response induction despite CRISPR-Cas protection. *Philos Trans R Soc Lond B Biol Sci* **380**, 20240474 (2025). https://doi.org/10.1098/rstb.2024.0474

69 Miezner, G. *et al.* An archaeal Cas3 protein facilitates rapid recovery from DNA damage. *Microlife* **4**, uqad007 (2023). https://doi.org/10.1093/femsml/uqad007

70 Fernandez-Garcia, L. *et al.* Toxin/antitoxin systems induce persistence and work in concert with restriction/modification systems to inhibit phage. *Microbiol Spectr* **12**, e0338823 (2024). https://doi.org/10.1128/spectrum.03388-23

71 Liu, J. & Gordon, B. R. Targeting the global regulator Lsr2 as a novel approach for anti-tuberculosis drug development. *Expert Rev Anti Infect Ther* **10**, 1049–1053 (2012). https://doi.org/10.1586/eri.12.86

72 Frunzke, J., Bramkamp, M., Schweitzer, J. E. & Bott, M. Population heterogeneity in Corynebacterium glutamicum ATCC 13032 caused by prophage CGP3. *Journal of Bacteriology* **190**, 5111–5119 (2008). https://doi.org/10.1128/jb.00310-08

73 Nanda, A. M. *et al.* Analysis of SOS-induced spontaneous prophage induction in Corynebacterium glutamicum at the single-cell level. *J Bacteriol* **196**, 180–188 (2014). https://doi.org/10.1128/JB.01018-13

74 Coluzzi, C., Garcillan-Barcia, M. P., de la Cruz, F. & Rocha, E. P. C. Evolution of Plasmid Mobility: Origin and Fate of Conjugative and Nonconjugative Plasmids. *Mol Biol Evol* **39** (2022). https://doi.org/10.1093/molbev/msac115

75 Doyle, M. *et al.* An H-NS-like stealth protein aids horizontal DNA transmission in bacteria. *Science* **315**, 251–252 (2007). https://doi.org/10.1126/science.1137550

76 Botelho, J. Defense systems are pervasive across chromosomally integrated mobile genetic elements and are inversely correlated to virulence and antimicrobial resistance. *Nucleic Acids Res* **51**, 4385–4397 (2023). https://doi.org/10.1093/nar/gkad282

77 Labrie, S. J., Samson, J. E. & Moineau, S. Bacteriophage resistance mechanisms. *Nat Rev Microbiol* **8**, 317–327 (2010). https://doi.org/10.1038/nrmicro2315

78 Tesson, F. & Bernheim, A. Synergy and regulation of antiphage systems: toward the existence of a bacterial immune system? *Curr Opin Microbiol* **71**, 102238 (2023). https://doi.org/10.1016/j.mib.2022.102238

79 Morin, L. M. C. *et al.* Why Do Filamentous Actinomycetota Produce Such a Vast Array of Specialized Metabolites? *Annu Rev Microbiol* **79**, 753–772 (2025). https://doi.org/10.1146/annurev-micro-060424-051257

80 Hamedi, J., Mohammadipanah, F. & Wink, J. 1 online resource (VII, 395 pages 380 illustrations, 341 illustrations in color (Springer International Publishing : Imprint: Springer,, Cham, 2017).

81 Bernheim, A. & Sorek, R. The pan-immune system of bacteria: antiviral defence as a community resource. *Nature Reviews Microbiology* **18**, 113–119 (2020). https://doi.org/10.1038/s41579-019-0278-2

82 Kensy, F., Zang, E., Faulhammer, C., Tan, R. K. & Buchs, J. Validation of a high-throughput fermentation system based on online monitoring of biomass and fluorescence in continuously shaken microtiter plates. *Microb Cell Fact* **8**, 31 (2009). https://doi.org/10.1186/1475-2859-8-31

83 Schafer, A. *et al.* Small mobilizable multi-purpose cloning vectors derived from the Escherichia coli plasmids pK18 and pK19: selection of defined deletions in the chromosome of Corynebacterium glutamicum. *Gene* **145**, 69–73 (1994). https://doi.org/10.1016/0378-1119(94)90324-7

84 Frunzke, J., Engels, V., Hasenbein, S., Gatgens, C. & Bott, M. Co-ordinated regulation of gluconate catabolism and glucose uptake in Corynebacterium glutamicum by two functionally equivalent transcriptional regulators, GntR1 and GntR2. *Molecular Microbiology* **67**, 305–322 (2008). https://doi.org/10.1111/j.1365-2958.2007.06020.x

85 Cremer, J., Eggeling, L. & Sahm, H. CLONING THE DAPA DAPB CLUSTER OF THE LYSINE-SECRETING BACTERIUM CORYNEBACTERIUM-GLUTAMICUM. *Molecular and General Genetics* **220**, 478–480 (1990). https://doi.org/10.1007/bf00391757

86 Livak, K. J. & Schmittgen, T. D. Analysis of relative gene expression data using real-time quantitative PCR and the 2(-Delta Delta C(T)) Method. *Methods* **25**, 402–408 (2001). https://doi.org/10.1006/meth.2001.1262

87 Benjamini, Y. & Hochberg, Y. Controlling the false discovery rate: a practical and powerful approach to multiple testing. *Journal of the Royal statistical society: series B (Methodological)* **57**, 289–300 (1995).

88 Petrosius, V. *et al.* Exploration of cell state heterogeneity using single-cell proteomics through sensitivity-tailored data-independent acquisition. *Nat Commun* **14**, 5910 (2023). https://doi.org/10.1038/s41467-023-41602-1

89 Demichev, V., Messner, C. B., Vernardis, S. I., Lilley, K. S. & Ralser, M. DIA-NN: neural networks and interference correction enable deep proteome coverage in high throughput. *Nat Methods* **17**, 41–44 (2020). https://doi.org/10.1038/s41592-019-0638-x

90 Kistner, F., Grossmann, J. L., Sinn, L. R. & Demichev, V. QuantUMS: uncertainty minimisation enables confident quantification in proteomics. *bioRxiv*, 2023.2006.2020.545604 (2023). https://doi.org/10.1101/2023.06.20.545604

91 Keppel, M. *et al.* HrrSA orchestrates a systemic response to heme and determines prioritization of terminal cytochrome oxidase expression. *Nucleic Acids Res* **48**, 6547–6562 (2020). https://doi.org/10.1093/nar/gkaa415

92 Helfrich, S. *et al.* Live cell imaging of SOS and prophage dynamics in isogenic bacterial populations. *Mol Microbiol* **98**, 636–650 (2015). https://doi.org/10.1111/mmi.13147

93 Grunberger, A. *et al.* A disposable picolitre bioreactor for cultivation and investigation of industrially relevant bacteria on the single cell level. *Lab Chip* **12**, 2060–2068 (2012). https://doi.org/10.1039/c2lc40156h

94 Grunberger, A. *et al.* Beyond growth rate 0.6: Corynebacterium glutamicum cultivated in highly diluted environments. *Biotechnol Bioeng* **110**, 220–228 (2013). https://doi.org/10.1002/bit.24616

95 Benson, D. A. *et al.* GenBank. *Nucleic Acids Res* **41**, D36–42 (2013). https://doi.org/10.1093/nar/gks1195

96 Goldfarb, T. *et al.* NCBI RefSeq: reference sequence standards through 25 years of curation and annotation. *Nucleic Acids Res* **53**, D243–D257 (2025). https://doi.org/10.1093/nar/gkae1038

97 Paysan-Lafosse, T. *et al.* The Pfam protein families database: embracing AI/ML. *Nucleic Acids Res* **53**, D523–D534 (2025). https://doi.org/10.1093/nar/gkae997

98 Eddy, S. R. Accelerated Profile HMM Searches. *PLoS Comput Biol* **7**, e1002195 (2011). https://doi.org/10.1371/journal.pcbi.1002195

99 Katoh, K. & Standley, D. M. MAFFT multiple sequence alignment software version 7: improvements in performance and usability. *Mol Biol Evol* **30**, 772–780 (2013). https://doi.org/10.1093/molbev/mst010

100 Minh, B. Q. *et al.* IQ-TREE 2: New Models and Efficient Methods for Phylogenetic Inference in the Genomic Era. *Mol Biol Evol* **37**, 1530–1534 (2020). https://doi.org/10.1093/molbev/msaa015

101 Paradis, E., Claude, J. & Strimmer, K. APE: Analyses of Phylogenetics and Evolution in R language. *Bioinformatics* **20**, 289–290 (2004). https://doi.org/10.1093/bioinformatics/btg412

102 Revell, L. J. phytools 2.0: an updated R ecosystem for phylogenetic comparative methods (and other things). *PeerJ* **12**, e16505 (2024). https://doi.org/10.7717/peerj.16505

103 Yu, G. Using ggtree to Visualize Data on Tree-Like Structures. *Curr Protoc Bioinformatics* **69**, e96 (2020). https://doi.org/10.1002/cpbi.96

104 Pfeifer, E. & Rocha, E. P. C. Phage-plasmids promote recombination and emergence of phages and plasmids. *Nat Commun* **15**, 1545 (2024). https://doi.org/10.1038/s41467-024-45757-3

105 Perez-Riverol, Y. *et al.* The PRIDE database at 20 years: 2025 update. *Nucleic Acids Res* **53**, D543–D553 (2025). https://doi.org/10.1093/nar/gkae1011

Supplementary Files

This is a list of supplementary files associated with this preprint. Click to download.

- 260416BadiaRoigeLsr2SupplementSubmission.pdf
- TableS3Annotation.xlsx
- TableS4Primers.xlsx
- TableS5Proteomics.xlsx
- TableS7RNASeqStatistics.xlsx
- TableS8lsr2genomes.xlsx
- TableS9lsr2regions.xlsx
- SuppVideo1minusCGP33h.avi
- SuppVIdeo2plusCGP33h.avi